LBL-32060
UC-000
Preprint

Lawrence Berkeley Laboratory

UNIVERSITY OF CALIFORNIA

EARTH SCIENCES DIVISION

Submitted to SPE Reservoir Engineering

The Laplace Transform Finite Difference (LTFD) Numerical Method for the Simulation of Compressible Liquid Flow in Reservoirs

G. Moridis, D.A. McVay, and D.L. Reddell

March 1992

For Reference

Not to be taken from this room

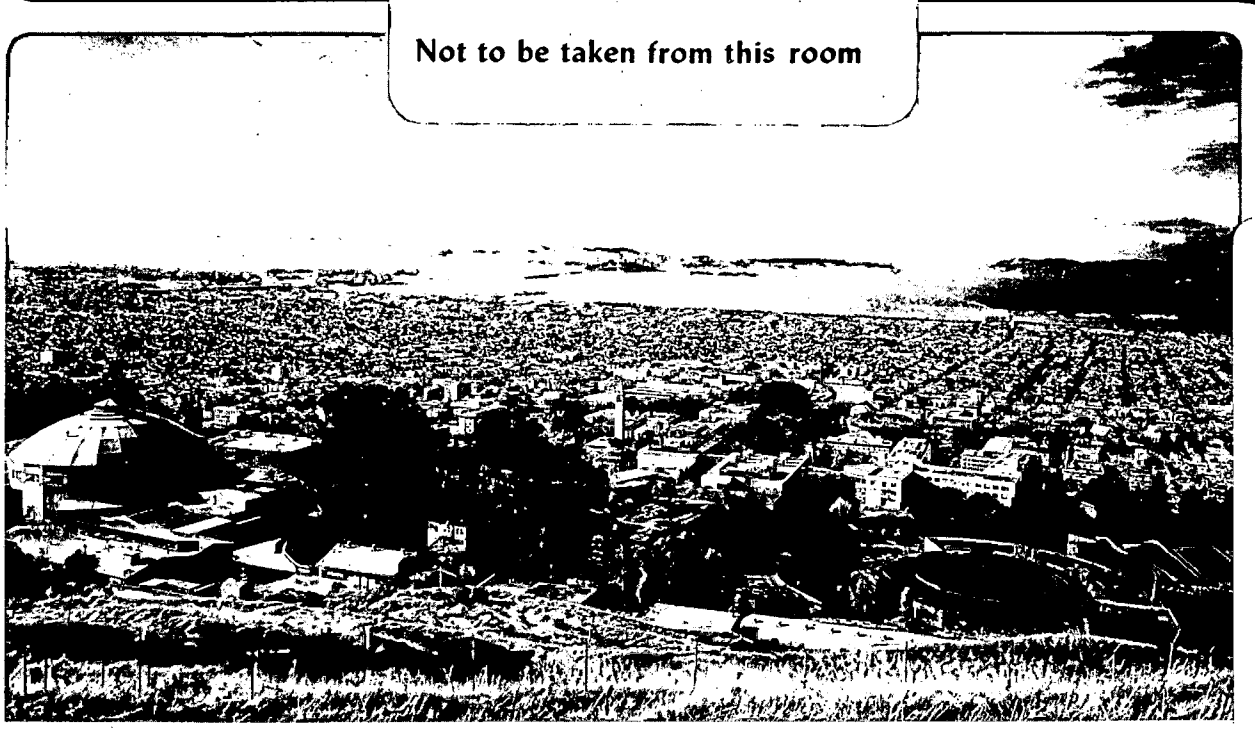

Prepared for the U.S. Department of Energy under Contract Number DE-AC03-76SF00098

LBL-32060
Copy 1
Bldg. 50 Library.

DISCLAIMER

This document was prepared as an account of work sponsored by the United States Government. While this document is believed to contain correct information, neither the United States Government nor any agency thereof, nor the Regents of the University of California, nor any of their employees, makes any warranty, express or implied, or assumes any legal responsibility for the accuracy, completeness, or usefulness of any information, apparatus, product, or process disclosed, or represents that its use would not infringe privately owned rights. Reference herein to any specific commercial product, process, or service by its trade name, trademark, manufacturer, or otherwise, does not necessarily constitute or imply its endorsement, recommendation, or favoring by the United States Government or any agency thereof, or the Regents of the University of California. The views and opinions of authors expressed herein do not necessarily state or reflect those of the United States Government or any agency thereof or the Regents of the University of California.

LBL-32060

The Laplace Transform Finite Difference (LTFD) Numerical Method for the Simulation of Compressible Liquid Flow in Reservoirs

G. Moridis,[*] D. A. McVay,[†] and D. L. Reddell[‡]

[*]Earth Sciences Division
Lawrence Berkeley Laboratory
University of California
Berkeley, California 94720

[†]Holditch & Assoc.
College Station, Texas 77843

[‡]Texas A & M University
College Station, Texas 77843

March 1992

This work was supported by the Texas Agricultural Experiment Station under Grant no. 6993/91 and by the U.S. Department of Energy under Contract No. DE-AC03-76SF00098.

The Laplace Transform Finite Difference (LTFD) Numerical Method for the Simulation of Compressible Liquid Flow in Reservoirs

G.J. Moridis* , SPE, Lawrence Berkeley Laboratory, **D.A. McVay,** SPE, S.A. Holditch & Assoc., and **D.L. Reddell,** Texas A&M U.

Abstract

A new numerical method, the Laplace Transform Finite Difference (LTFD) method, was developed for the simulation of single-phase compressible liquid flow through porous media in one, two or three dimensions. The major advantage of LTFD is that it eliminates time dependency, the need for time discretization, and the problems stemming from the treatment of the time derivative in the nonlinear equation of flow by employing a Laplace transform formulation. The LTFD method yields a solution semi-analytical in time and numerical in space, and renders the effects of the time derivative on accuracy and stability irrelevant because time is no longer a consideration. The method was tested against results from one-, two- and three-dimensional test cases obtained from a standard Finite Difference (FD) simulator, as well as from analytical models. For a single timestep, LTFD requires an execution time 6 to 10 times longer than the analogous FD requirement without an increase in storage. However, this disadvantage is outweighed by the fact that LTFD allows an unlimited timestep size. Execution times may be reduced by orders of magnitude because calculations in the LTFD scheme are necessary only at the desired observation times, while in a standard FD method calculations are needed at all the intermediate times

* Formerly at Texas A& M U.

of the discretized time domain. Thus, a problem in standard FD format may require several hundred timesteps and matrix inversions between the initial condition and the desired solution time, but LTFD requires only one timestep and no more than 6 to 10 matrix inversions. Moreover, LTFD yields a stable, non-increasing material balance error in addition to a more accurate solution than the conventional FD.

Introduction

In transient flow through porous media, the general Partial Differential Equation (PDE) to be solved is obtained by combining appropriate forms of Darcy's Law and the equation of mass conservation, yielding:

$$\nabla \cdot \left[k \frac{\rho}{\mu} \left(\nabla p - \rho g \nabla z \right) \right] = \frac{\partial}{\partial t} (\rho \phi) + \tilde{q}. \tag{1}$$

Eq. 1 is generally nonlinear and contains the time derivative $\partial p / \partial t$, of which the numerical approximation is consistently the most important source of instability and error in numerical models. The treatment of $\partial p / \partial t$ in a traditional Finite Difference (FD) approximation scheme involves the discretization of the continuous time coordinate into a large number of small timesteps Δt. Numerical solutions at a number of representative points κ in the domain are then sought at the discrete times

$$t_0 = 0, \; t_1 = \Delta t_1, \; t_2 = \Delta t_1 + \Delta t_2, \ldots, t_n = \sum_{\ell=1}^{n} \Delta t_\ell \; , \tag{2}$$

where the dependent variable $p_\kappa(t)$ is approximated by a set of values $\tilde{p}_\kappa^\ell$, $\ell = 1, 2, \ldots n$. The PDE problem with a continuous smooth solution surface is thus reduced to a set of algebraic equations relating the discrete approximate values $\tilde{p}_\kappa$ to each point κ. A Taylor series approximation of the time derivative yields

$$\left(\frac{\partial p_\kappa}{\partial t} \right)^\nu = \frac{1}{\Delta t_{n+1}} \left(\tilde{p}_\kappa^{n+1} - \tilde{p}_\kappa^n \right) + E_{\kappa,n} \; , \tag{3}$$

where

$$E_{\kappa,n} = p''_{\kappa}\frac{\Delta t_{n+1}}{2} - p'''_{\kappa}\frac{\Delta t^2_{n+1}}{6} + \cdots \tag{4}$$

is the truncation error, and $n+1$ and n denote the current time and previous times of the discretized time domain. For $\nu = n$, Eq. 3 represents a forward difference approximation and results in the explicit formulation of the FD, which is not unconditionally stable; for $\nu = n+1$, Eq. 3 represents a backward difference approximation and results in the unconditionally stable implicit formulation of the FD. The above approximation introduces an error of order $O(\Delta t)$. Accuracy (and, in the case of the explicit formulation, stability) considerations preclude the use of a large Δt. Minimization of $E_{\kappa,n}$ often dictates the use of a large number of small timesteps Δt between desired observation times, requiring longer execution times and resulting in potentially larger roundoff errors. The problem of restriction on the size of Δt is further exacerbated by the nonlinearity of the PDE, which is caused by the pressure dependence of the liquid density and the formation porosity. This necessitates even shorter timesteps, dictates internal iterations within each timestep until a convergence criterion is met, and adds significantly to the computational load.

The Laplace Transform Finite Difference (LTFD) method belongs to a family of new, Laplace transform-based numerical methods recently introduced by Moridis and Reddell[1-5]. It was first applied to the solution of the diffusion-type (parabolic) PDE of incompressible flow through porous media[1,2], and was extended to the solution of the advection-diffusion (hyperbolic) PDE of solute transport (miscible displacement) in porous media[3]. The major advantage of LTFD is that it eliminates the time dependency of the problem because of the Laplace transform formulation employed, and thus the need for time discretization for an accurate, stable solution. In essence, LTFD yields a solution semi-analytical in time and numerical in space. An unlimited Δt size is possible without loss of accuracy or stability, and the need for a large number of intermediate steps between

desired observation times is eliminated.

In the present paper, the LTFD method was formulated to address the problem of slightly compressible, single-phase liquid flow through porous media. The mathematical basis of the method is developed, and its performance is evaluated against analytical solutions and standard FD models.

The Nonlinear Liquid Flow Equation

A general equation for liquid density is[6]

$$\rho = \rho_{STC}\beta, \quad \beta = \beta_0\ R, \quad R = \exp[C_L(p - p_0)]\ , \tag{5}$$

where β is the inverse of the formation volume factor. Then

$$p = p_0 + \frac{1}{C_L}\ln\left(\frac{\rho}{\rho_0}\right) = p_0 + \frac{1}{C_L}\ \ln\left(\frac{\beta}{\beta_0}\right) = p_0 + \frac{1}{C_L}\ \ln R\ , \tag{6}$$

where $\rho_0 = \rho_{STC}\beta_0$. Differentiation of Eq. 6 yields

$$\frac{\partial p}{\partial d^\circ} = \frac{1}{C_L}\ \frac{1}{R}\ \frac{\partial R}{\partial d^\circ}, \qquad \frac{\partial p}{\partial R} = \frac{1}{C_L}\ \frac{1}{R}, \tag{7}$$

where $d^\circ \equiv x$,y, z in cartesian coordinates, or $d^\circ \equiv r$, θ, z in cylindrical coordinates.

Expansion of the left-hand side of Eq. 1 and substitution for p yields

$$\frac{\partial}{\partial d^\circ}\left[k\frac{\rho}{\mu}\ \left(\frac{\partial p}{\partial d^\circ} - \rho g\frac{\partial z}{\partial d^\circ}\right)\right]$$

$$= \frac{\partial}{\partial d^\circ}\left[k\frac{\rho_0}{\mu C_L}\ \frac{\partial R}{\partial d^\circ} - \frac{k}{\mu}\ g\rho_0^2 R^2 z_{d^\circ}\right]\ , \tag{8}$$

where z_{d° is the elevation gradient along the d° direction.

Expansion of the time derivative in the right-hand side of Eq. 1 and substitution for ρ and $\partial p/\partial R$ yields

$$\frac{\partial}{\partial t}(\rho\phi) = \rho_0\left(\phi + R\ \frac{\partial\phi}{\partial p}\ \frac{\partial p}{\partial R}\right)\frac{\partial R}{\partial t} = \rho_0 C_T\frac{\partial R}{\partial t}\ , \tag{9}$$

where $C_T = \phi + (1/C_L)(\partial\phi/\partial p)$.

The porosity ϕ is a weak function of pressure. For consolidated formations the variation of pore volume with pressure is accounted for by[6]

$$\phi = \phi_0 \exp[C_R(p - p_0)] \ . \tag{10}$$

From Eqs. 6 and 10,

$$\phi = \phi_0 \ R^{(C_R/C_L)}, \quad \frac{\partial\phi}{\partial p} = \phi_0 \ C_R \ R^{(C_R/C_L)} \ , \tag{11}$$

leading to

$$C_T = \phi_0 \left(1 + \frac{C_R}{C_L}\right) R^{(C_R/C_L)} \ . \tag{12}$$

For large pressure differentials of compressible liquids in compressible reservoirs, $R \neq 1$ and Eq. 12 has to be used in its most general form. For small pressure differentials, $R \simeq 1$ and C_T is reduced to the constant

$$C_T \simeq \phi_0 \left(1 + \frac{C_R}{C_L}\right) \ . \tag{13}$$

For nearly incompressible formations $C_T \simeq \phi_0$.

Substitution in Eq. 1 and division by the constant ρ_0 yields the general equation of compressible liquid flow in cartesian coordinates as

$$\begin{aligned} &\frac{\partial}{\partial x}\left[\frac{k_x}{\mu C_L}\frac{\partial R}{\partial x} - \frac{k_x}{\mu}\, g z_x \rho_0 R^2\right] \\ &+ \frac{\partial}{\partial y}\left[\frac{k_y}{\mu C_L}\frac{\partial R}{\partial y} - \frac{k_y}{\mu}\, g z_y \rho_0 R^2\right] \\ &+ \frac{\partial}{\partial z}\left[\frac{k_z}{\mu C_L}\frac{\partial R}{\partial z} - \frac{k_z}{\mu}\, g z_z \rho_0 R^2\right] = C_T \frac{\partial R}{\partial t} + q \ , \end{aligned} \tag{14}$$

where $q = \tilde{q}/\rho_0$. In cylindrical coordinates

$$\frac{1}{r}\frac{\partial}{\partial r}\left[r \ \frac{k_r}{\mu C_L}\frac{\partial R}{\partial r}\right] + \frac{1}{r^2}\frac{\partial}{\partial \theta}\left[\frac{k_\theta}{\mu C_L}\frac{\partial R}{\partial \theta}\right]$$

$$+\frac{\partial}{\partial z}\left[\frac{k_z}{\mu C_L}\,\frac{\partial R}{\partial z}-\frac{k_z}{\mu}\,g z_z \rho_0 R^2\right]=C_T\,\frac{\partial R}{\partial t}+q\,. \tag{15}$$

Inspection of the R formulation of Eqs. 14 and 15 reveals the following:

1. The nonlinearity of the product $\rho\partial p/\partial d^\circ$, ($d^\circ \equiv x,\ y,\ z$ in cartesian coordinates, or $d^\circ \equiv r,\ \theta,\ z$ in cylindrical coordinates) in the original PDE (Eq. 1) has been removed.

2. The nonlinearity of ρ^2 in the gravitational components is maintained in R^2.

3. For areal simulations and all cases where gravitational effects are not included, the flow Eqs. 14 and 15 are linear if C_T can be approximated by Eq. 13 within a desired degree of accuracy.

4. When gravity effects are included or C_T cannot be adequately described by Eq. 13, Eqs. 14 and 15 are weakly nonlinear.

Eqs. 14 and 15 are theoretically correct, but present potentially serious computational problems which severely limit the usefulness of the R formulation even if the nonlinearity in R^2 is not considered. If solutions in terms of R are sought, near-singular matrices result almost invariably. Such behavior is more pronounced if the pressure changes are small. This is caused by (a) the inherent machine accuracy limitations, and (b) the proximity of R to the value of 1 and its relative insensitivity even to very significant pressure variations, due to the small compressibility of the reservoir liquids. Significant changes in pressure (thousands of psi) may result in minuscule decreases in R which may vary within a narrow range (i.e. between 0.95 and 1). Solutions in R may thus suffer from substantial errors.

These problems of nonlinearity and nonsingularity are alleviated by reformulating Eqs. 14 and 15 in terms of ΔR, i.e. the deviation of R from the value of 1 corresponding to the reference pressure p_0. Substitution for

$$R=1+\Delta R,\quad R^2=1+2\cdot\Delta R+(\Delta R)^2 \tag{16}$$

in Eqs. 14 and 15 yields

$$\begin{aligned}
&\frac{\partial}{\partial x}\left[\lambda_{x1}\,\frac{\partial(\Delta R)}{\partial x}-\lambda_{x2}\left[1+2\cdot\Delta R+(\Delta R)^2\right]\right]\\
&+\frac{\partial}{\partial y}\left[\lambda_{y1}\,\frac{\partial(\Delta R)}{\partial y}-\lambda_{y2}\left[1+2\cdot\Delta R+(\Delta R)^2\right]\right]\\
&+\frac{\partial}{\partial z}\left[\lambda_{z1}\,\frac{\partial(\Delta R)}{\partial z}-\lambda_{z2}\left[1+2\cdot\Delta R+(\Delta R)^2\right]\right]=C_T\,\frac{\partial(\Delta R)}{\partial t}+q\ ,
\end{aligned}\tag{17}$$

in cartesian coordinates, and

$$\begin{aligned}
&\frac{1}{r}\,\frac{\partial}{\partial r}\left[r\,\lambda_{r1}\,\frac{\partial(\Delta R)}{\partial r}\right]+\frac{1}{r^2}\,\frac{\partial}{\partial\theta}\left[\lambda_{\theta 1}\,\frac{\partial(\Delta R)}{\partial\theta}\right]\\
&+\frac{\partial}{\partial z}\left[\lambda_{z1}\,\frac{\partial(\Delta R)}{\partial z}-\lambda_{z2}\left[1+2\,\Delta R+(\Delta R)^2\right]\right]=C_T\,\frac{\partial(\Delta R)}{\partial t}+q
\end{aligned}\tag{18}$$

in cylindrical coordinates, where

$$\lambda_{d^\circ 1}=\frac{k_{d^\circ}}{\mu\,C_L}\quad\text{and}\quad\lambda_{d^\circ 2}=\frac{k_{d^\circ}}{\mu}\,g\,z_{d^\circ}\,\rho_0\ ,\tag{19}$$

and $d^\circ \equiv x, y, z$ or r, θ, z. Eqs. 17 and 18 are the fundamental equations of flow of compressible liquids through porous media in their most general form.

The LTFD Numerical Method

The Laplace Transform Finite Difference (LTFD) numerical method eliminates the accuracy and stability problems caused by the treatment of the time derivative in Eq. 1 by providing a numerical solution in the Laplace space. This approach renders time considerations and limitations irrelevant. The vector of the unknowns in time is then obtained by numerically inverting the Laplace-space solution using the Stehfest algorithm[7,8]. The numerical simulation of nonlinear (compressible) liquid flow using the LTFD method consists of four steps described in detail in the following sections.

Step 1: The Laplace Transform of the PDE. The Laplace transform of Eq. 17 yields

$$\begin{aligned}
&\frac{\partial}{\partial x}\left[\lambda_{x1}\,\frac{\partial\Psi}{\partial x} - \lambda_{x2}\cdot C_\beta\;\Psi - \lambda_{x2}\cdot\frac{1}{s}\right] \\
&+\frac{\partial}{\partial y}\left[\lambda_{y1}\,\frac{\partial\Psi}{\partial y} - \lambda_{y2}\;C_\beta\;\Psi - \lambda_{y2}\;\frac{1}{s}\right] \\
&+\frac{\partial}{\partial z}\left[\lambda_{z1}\,\frac{\partial\Psi}{\partial z} - \lambda_{z2}\;C_\beta\;\Psi - \lambda_{z2}\;\frac{1}{s}\right] = C_T\;\left[s\;\Psi - \Delta R(0)\right] + \ddot{q}\;,
\end{aligned} \tag{20}$$

where s is the Laplace space parameter, $\Delta R(0)$ is the distribution of ΔR at $t = 0$,

$$C_\beta = 2 + \overline{\Delta R}\;, \tag{21}$$

$$\ddot{q} = \mathcal{L}\{q\}\;, \tag{22}$$

and

$$\Psi = \mathcal{L}\{\Delta R\}\;, \tag{23}$$

with $\mathcal{L}\{\}$ denoting the Laplace transform of the quantity in braces. The q in Eq. 20 does not have to be time-invariant since Eq. 22 is general and allows the transformation of any time-variable $q(t)$ which has a Laplace transform.

Applying the same procedures to a three-dimensional cylindrical coordinate system yields the following equation in the Laplace space:

$$\begin{aligned}
&\frac{1}{r}\,\frac{\partial}{\partial r}\left[r\;\lambda_{r1}\;\frac{\partial\Psi}{\partial x}\right] + \frac{1}{r^2}\,\frac{\partial}{\partial\theta}\left[\lambda_{\theta 1}\;\frac{\partial\Psi}{\partial x}\right] \\
&+\frac{\partial}{\partial z}\left[\lambda_{z1}\;\frac{\partial\Psi}{\partial z} - \lambda_{z2}\;C_\beta\;\Psi - \lambda_{z2}\;\frac{1}{s}\right] = C_T\;\left[s\;\Psi - \Delta R(0)\right] + \ddot{q}\;.
\end{aligned} \tag{24}$$

The term C_β is obtained from the linearization of

$$2\;\Delta R + (\Delta R)^2 = (2 + \Delta R)\;\;\Delta R \simeq C_\beta\;\Delta R$$

over the interval from $t = 0$ to $t = t$, and

$$\overline{\Delta R} = (1/t)\int_0^t \Delta R\;dt = (1/t)\mathcal{L}^{-1}\{\Psi/s\}\;. \tag{25}$$

If small pressure differentials are involved, the approximation $C_\beta \simeq 2$ can be used with negligible effects on accuracy.

Step 2: The FD Scheme in the Laplace Space. We employed a "block centered" grid[6] method in the space discretization of the transformed PDE. In this paper, the subscript i, j, k refer to the position in the three-dimensional grid, and define the ith, jth and kth grid-block center in the x, y and z direction respectively, with $i = 1, \ldots, MX$, $j = 1, \ldots, MY$ and $k = 1, \ldots, MZ$. The parameters MX, MY and MZ are the number of subdivisions of the x, y and z coordinate. This discretization divides the solution space into $N_T = MX \times MY \times MZ$ locally uniform and homogenous grid-blocks.

Using a FD scheme with an appropriate space discretization, truncation errors are minimized and the continuous three-dimensional PDE's (Eqs. 20 and 24) in the Laplace space are approximated by (and reduced to) the following algebraic form (see Appendix):

$$\begin{aligned} &AX\ \Psi_{i-1} + BX\ \Psi + CX\ \Psi_{i+1} + GX \\ &+AY\ \Psi_{j-1} + BY\ \Psi + CY\ \Psi_{j+1} + GY \\ &+AZ\ \Psi_{k-1} + BZ\ \Psi + CZ\ \Psi_{k+1} + GZ = C_T\ [s\ \Psi - \Delta R(0)] + \ddot{q}\ . \end{aligned} \tag{26}$$

For simplicity, the subscripts i, j, and k are omitted and only those needed to illustrate communication between gridblocks are mentioned.

Collecting and rearranging terms, the final form of the FD equation in the Laplace space is

$$\begin{aligned} &AX\ \Psi_{i-1} + AY\ \Psi_{j-1} + AZ\ \Psi_{k-1} + B \\ &+ CX\ \Psi_{i+1} + CY\ \Psi_{j+1} + CZ \cdot \Psi_{k+1} = D\ , \end{aligned} \tag{27}$$

where

$$B = BX + BY + BZ - C_T \cdot s\ , \tag{28}$$

$$D = -C_T\ \Delta R(0) + \ddot{q} + GG\ , \tag{29}$$

and

$$GG = -(GX + GY + GZ) \ . \tag{30}$$

Step 3: The Solution in the Laplace Space. The FD approximation of the partial differential equations over the solution domain (x, y, z) or (r, θ, z) in the Laplace space results in N_T simultaneous equations. Written in matrix notation, the FD system of simultaneous equations in Eq. 27 becomes

$$\mathbf{M}\ \vec{\Psi} = \vec{D} \ , \tag{31}$$

where $\mathbf{M}$ is the flow coefficient matrix, $\vec{\Psi}$ is the vector of the unknown transformed ΔR's, and $\vec{D}$ the 'known' right-hand side vector.

The solution of Eq. 31 necessitates computation of $\mathbf{M}$ and $\vec{D}$, and requires arithmetic values of the s parameter of the Laplace space. For a desired observation time t, these are provided by the first part of the Stehfest algorithm[7,8] as

$$s_\nu = \frac{\ln 2}{t}\nu \ , \quad \nu = 1, \ldots, N_S \ , \tag{32}$$

where N_S is the number of summation terms in the algorithm and N_S is an even number. Optimum values for N_S were discussed extensively by Moridis and Reddell[1,2]. Solution of Eq. 31 returns the set of N_S vectors

$$\vec{\Psi}_\nu = \mathbf{M}_\nu^{-1}\ \vec{D}_\nu \ , \quad \nu = 1, \ldots, N_S \ . \tag{33}$$

To obtain a solution at a time t, all vectors $\vec{\Psi}_\nu$, $\nu = 1, \ldots, N_S$ are needed, i.e. the system of simultaneous equations has to be solved N_S times.

Step 4: The Numerical Inversion of the Laplace Solution. The unknown vector $\overrightarrow{\Delta R}$ at time t is obtained by using the Stehfest algorithm[7,8] to numerically invert the Laplace

solutions $\vec{\Psi}_\nu$. The procedure is described by the following equations:

$$\overrightarrow{\Delta R}(t) = \frac{\ln 2}{t} \sum_{\nu=1}^{N_S} W_\nu \cdot \vec{\Psi}_\nu \ , \tag{34}$$

and

$$W_\nu = F_\nu \sum_{\kappa=L_0}^{L_M} \frac{\kappa^{\frac{N_S}{2}}(2\kappa)!}{(\frac{N_S}{2}-\kappa)!\kappa!(\kappa-1)!(\nu-\kappa)!(2\kappa-\nu)!} \ , \tag{35}$$

where $F_\nu = (-1)^{\frac{N_S}{2}+\nu}$, $L_0 = \frac{1}{2}(\nu+1)$, and $L_M = \min\{\nu, \frac{N_S}{2}\}$. $\vec{R}$ is then computed as

$$\vec{R}(t) = \vec{I} + \overrightarrow{\Delta R}(t) \ , \tag{36}$$

where $\vec{I}$ is the unit vector. The pressure vector $\vec{p}$ can be obtained from Eq. 6.

Although the accuracy of the method is theoretically expected to improve with increasing N_S, Stehfest[7] indicated that with increasing N_S the number of correct significant figures inreases linearly at first and then, due to roundoff errors, decreases linearly. Testing his algorithm against 50 equations with known inverse Laplace transforms, he determined the optimum $N_S = 10$ for single precision variables (8 significant figures) and $N_S = 18$ for double precision variables (16 significant figures). Investigating the performance of LTFD in the simulation of flow of incompressible fluids, Moridis and Reddell[1,2] determined that optimum results were obtained for a N_S between 16 and 20, but that the improvement in accuracy between $N_S = 8$ and $N_S = 20$ was marginal.

The use of steep time functions for time-variable well rates and boundary conditions (i.e. step functions or pulses) poses no conceptual and mathematical problem in the Laplace space. The presence of such steep functions may reduce the accuracy of the solution because of limitations of the inversion algorithm. In this case the value of N_S needed for a sufficiently accurate solution rises to $18 \leq N_S \leq 24$. Although at such a high N_S some oscillations still persist in the immediate vicinity of the time t_s at which the step function or pulse occurs, we determined that these affect the solution by less than 1%, completely disappear for $t \geq 1.15t_s$, and have a negligible effect on the mass balance error.

The solution in the Laplace space eliminates the stability and accuracy problems caused by the treatment of the time derivative in standard FD simulators, thus allowing an unlimited timestep size. In a standard FD method, there are three sources of error: the time-related truncation error, the space-related truncation error, and the roundoff error. Because the time domain is not discretized, there is no time-related truncation error in the LTFD method, in which the sources of error are the truncation error caused by the space discretization, the error attributed to the numerical inversion of the Laplace solution, and the roundoff error. The numerical inversion creates very little (if any) error, which for smooth time functions can be at the level of machine accuracy. The ability to use an unlimited timestep size bounds the accumulation of roundoff error by an upper limit defined as the roundoff error accumulated after the N_S solutions required by the method. Thus, the LTFD solution is inherently more accurate than the standard FD method for the same grid system. It offers a stable, non-increasing roundoff error irrespective of the time of observation t_{obs} because calculations have to be performed at this time only using a $\Delta t = t_{obs}$; on the other hand, calculations in a standard FD method have to be performed at all the intermediate times

$$(t_{int})_i = \sum_{i=1}^{\ell} \Delta t_i, \quad \ell = 1, 2, \ldots, L \quad \text{and} \quad \sum_{i=1}^{L} = t_{obs} \ , \tag{37}$$

continuously accumulating roundoff error in the process.

The LTFD method does not increase the memory requirements over a standard FD method because a) the values of the unknowns at the previous time step are not needed, since no intermediate timesteps are necessary, and the Δ size coincides with the observation time, and b) the N_S sets of unknowns can be stored and summed in a single array. In the FD method this array is that of the unknowns at the end of the previous timestep.

Inner Iterations. These are required only when the approximations of C_T in Eq. 13

and of C_β in Eq. 21 are not acceptably accurate. Under these circumstances, the LTFD method is easily extended to cover these weak nonlinearities through an iteration procedure entirely analogous to the treatment of such nonlinearities in FD. The process involves a limited number of inner iterations (2 to 4), during which the values of C_T and C_β are updated and an improved solution ΔR is obtained until a desired convergence criterion is met.

Verification and Test Problems

The LTFD numerical method was tested using four test problems which represented increasing levels of complexity. Analytical solutions exist for the first two problems. The LTFD solution was verified through comparison with the analytical solutions. No analytical solutions exist for the other two test problems. In all four cases the results obtained with LTFD were tested against results obtained using a standard, commercially available implicit FD simulator[9] with the same space discretization. A direct banded-matrix solver was used to solve the system of simultaneous equations arising in both the LTFD and FD methods. Double precision variables with 16 and 20 significant figures were used in all simulations. A variable timestep Δt was used for all test cases in the FD simulator, given by the recursive formula

$$\Delta t_\ell = \min\{M_L \times \Delta t_{\ell-1}, \Delta t_{max}, \Delta t_{\Delta pmax}\} \tag{38}$$

where M_L is a multiplier, Δt_{max} is the maximum permissible Δt, and $\Delta t_{\Delta pmax}$ is the Δt corresponding to a maximum permissible pressure change Δp_{max}. Table 1 shows the M_L, Δt_0, Δt_{max}, and Δp_{max} used in the four test problems, as well as the number of timesteps and matrix solutions (i.e. the number of times the system of simultaneous equations in the FD simulator had to be solved) in the simulations. Because of internal iterations, the number of matrix solutions is significantly larger than the number of timesteps.

Verification and Test Problem 1. Test Problem 1 was a problem of flow to a well in a circular bounded reservoir, for which a number of exact and approximate analytical solutions exist. **Table 2** shows the fluid properties. Reservoir properties and dimensions, and discretization information for the FD and LTFD simulations appear in **Table 3.** We used the equation provided by vanEverdingen and Hurst[10] for the computation of the analytical solutions.

We investigated three subproblems. In Problem 1a we compared the LTFD and the analytical solutions over the whole reservoir at 4 observation times. We used $N_S = 8$ in all the LTFD simulations of Problem 1a. **Fig. 1** shows that the two solutions coincided regardless of the magnitude of observation time. This gives the measure of the accuracy of LTFD, and shows the complete insensitivity of the method to the size of the time increment.

In Problem 1b we compared the LTFD solution with $N_S = 8$ to a) the analytical solution, and b) 4 FD solutions (see **Table 1**) for t = 60 days. **Fig. 2** shows in a dimensionless formulation the percent difference between the analytical and the numerical solutions. The LTFD solution exhibited a very small deviation from the analytical solution, and was consistently superior to the FD difference solution. The superiority of LTFD persisted even when a very fine time discretization (65 timesteps, and a total of 136 matrix solutions) was used in the FD simulation, indicating that for 1/17th of the computational load (8 vs 136) LTFD returned a more accurate solution than the FD. With an increasing number of timesteps (corresponding to smaller Δt's, the FD solutions tended asymptotically towards the analytical and the LTFD solutions.

In Problem 1c we studied the effect of N_S on the performance of LTFD. For a N_S ranging between 6 and 20, we observed a negligible difference between the analytical and the LTFD solutions (**Fig. 3**) at t = 1000 days. The minimum absolute difference was observed for $N_S = 6$, and increased with an increasing N_S until $N_S = 12$. The solutions for an N_S between 12 and 20 were identical and exhibited arithmetic differences in the

7th decimal place and beyond.

The implications of the results in **Fig. 3** are that a) the accuracy of LTFD for this one-dimensional problem is practically insensitive to the value of N_S, and b) the number of summation terms N_S for an accurate solution may be 6, far smaller than the $N_S = 18$ which Stehfest[7] suggested for double precision variables. This drastically reduces the execution time and makes the LTFD method even more efficient than theoretically predicted.

Verification and Test Problem 2. Test Problem 2 involved flow towards a well at the center of a bounded square reservoir with an infinite-conductivity vertical fracture at the center of the square. The fluid properties remain as in Test Problem 1. **Fig. 4** shows the reservoir geometry, and **Table 4** presents reservoir properties and dimensions, and the grid discretization used in the FD and LTFD simulations. We used the analytical solution of Gringarten *et al*[11] (which predicts the unsteady-state pressure at the well) as a reference. We investigated two subproblems.

In Problem 2a we compared the LTFD and analytical solutions at the well for 9 observation times. We let $N_S = 8$ in the LTFD simulations. We observed a pattern similar to the one in Test Problem 1. The two solutions coincided regardless of the magnitude of observation time (**Fig. 5**). This testifies to the power and accuracy of LTFD, and confirms the complete insensitivity of the method to the size of the time increment.

Analytical solutions of the pressure distribution in the formation do not exist for this problem. In Problem 2b we compared the LTFD solution ($N_S = 8$) to 4 FD solutions along the y axis at $x = 0.025$ ft at t =365 days. **Fig. 6** shows in a dimensionless formulation the difference between the LTFD and the FD solutions. We observed an identical pattern: with an increasing number of Δt's the FD solutions a) tended to the LTFD solution, and consequently b) the difference between the two solutions decreased. Using a very fine time discretization (79 timesteps, and a total of 231 matrix solutions), the FD yielded a solution

within 0.1 psi of the LTFD solution, but with a computational load 29 times larger.

In Problem 2c we studied the effect of N_S on the performance of LTFD along the same axis and at the same time. In **Fig. 7** we show the absolute difference between the LTFD solutions for different N_S values from a reference, taken as the solution obtained with $N_S = 8$. A slightly different pattern emerged. With the exception of $N_S = 6$, all other solutions exhibited extremely small pressure differences from each other, i.e. 0.1 to 0.2 psi when p was in excess of 3000 psia. The solution for $N_S = 6$ was consistently about 5 psi higher than the rest of the solutions, which, while significantly larger than all the other deviations, was still very small when compared to the maximum pressure change of 1835 psi. In light of the significant difference in the computational load, a $N_S = 6$ could easily be used when extreme accuracy is not essential. These results confirm our previous observations that the accuracy of LTFD is virtually insensitive to the value of N_S for $8 \leq N_S \leq 20$. Slightly lower accuracy (insignificant for most practical applications) may be obtained for $N_S = 6$.

Test Problem 3. Test Problem 3 was a two-dimensional (areal) simulation problem, and represented a reservoir with spatially variable properties and wells with variable flow rates. The fluid properties remain the same as in Test Problem 1. The reservoir geometry, formation thickness, and permeability distribution are depicted in the contour plots of **Fig. 8**. Reservoir properties, dimensions, and discretization information are in **Table 5**. **Table 6** lists the production rates for the 10 wells in the reservoir, of which 3 have constant rates, 3 have linearly declining (with time) rates, and 4 have exponentially declining rates. No analytical solution is available for this problem. A comparison of the LTFD and the FD solutions provided a measure of the power, validity and accuracy of the LTFD method.

Fig. 9 shows of the pressure distribution in the reservoir for the LTFD solution ($N_S = 8$) at t = 180 days. We evaluated LTFD by comparing the pressure distribution

along the x axis at $y = 2900$ ft, corresponding to row $J = 15$ (**Fig. 10**). The accuracy of the LTFD solution was indicated by the fact that for a decreasing Δt (which results in smaller truncation errors, more accurate solutions, and larger numbers of timesteps) the FD solution tended to approach the LTFD solution and the difference between the two solutions decreased. For 86 timesteps, a total of 329 matrix solutions, and 41 times the computational load of LTFD, the FD solution virtually coincides with the LTFD solution. FD cannot deliver the accuracy of LTFD unless a very large number of timesteps is taken, and then only at the expense of significantly increased CPU time. **Fig. 10** demonstrates that LTFD can capture in detail the significant pressure changes due to the presence of wells and zones of different permeability. The well locations and permeability zones can be identified by the existence of peaks and sharp variations in drawdown. These variations decrease in magnitude with a decreasing Δt size in the FD solution. For large Δt's, the FD solutions exhibited significant deviations and insufficient accuracy. This was caused by the averaging effect used in the treatment of the time derivative. With smaller Δt's, these deviations decreased, and the accuracy of FD the solution improved.

Test Problem 4. In the three-dimensional Test Problem 4, we studied a horizontal well in an anisotropic reservoir. Due to symmetry, we simulated only 1/8th of the reservoir volume (**Fig. 11**). The fluid properties remain as in Test Problem 1. We provide information on the reservoir properties, dimensions, and discretization in **Table 6**. As in Test Problem 3, we evaluated LTFD ($N_S = 8$) by comparing results with 5 FD simulations. We compared pressure distributions a) along the x axis at z = 0.125 ft (K=2), y = 0.125 ft (J=2), and b) at the xy plane at z = 0.125 ft (K=2).

We present the pressure distributions, as well as the difference between the two solutions, in **Figs. 12 and 13**. The same pattern observed in all previous test cases is obvious: LTFD produced an accurate solution, a fact indicated by the realization that the

FD solution for a decreasing Δt size (which results in smaller truncation errors, more accurate solutions, and larger numbers of timesteps) a) tended to the LTFD solution, and consequently b) the difference between the two solutions decreased and tended to zero. The LTFD solution at t=1000 days is virtually identical to the FD solution with 231 timesteps and 680 matrix solutions (**Figs. 12a and 13a**). The percent absolute difference between the two solutions in **Figs. 12b and 13b** do not exceed 0.021%, which corresponds to a maximum difference of 0.5 psi at the pressure of the reservoir. LTFD is capable of delivering (and exceeding) the accuracy of a FD solution with an extremely small time discretization, but without the corresponding computational load. Significant accelerations (by a factor of 85 in this case) of solution times by orders of magnitude are thus possible.

Material Balance Error Considerations. A very important measure of the validity and accuracy of the LTFD numerical method was provided by the magnitude of the material balance error as a percentage of the original fluid mass. **Fig. 14** shows an analysis of the behavior of the material balance errors for the four Test Problems for both the LTFD and the FD methods. The small magnitude (bordering machine precision) of the material balance error for the methods shows that they both conserve mass. The extremely small magnitude of the LTFD material balance error further testified to the power of the method. LTFD seemed to have an overall advantage over FD, indicated by the generally lower material balance errors. With the condititional exception of the computationally simple Test Problem 1, LTFD produced consistently a smaller error. This was more obvious in the more difficult problems 3 and 4. The ΔR formulation may be conceptually powerful, but it poses some computational difficulties since it involves solving matrices with coefficients that vary by up to 8 orders of magnitude. In small problems, LTFD will produce a very accurate solution, but the roundoff error involved may make FD infinitesimally more accurate (i.e. by the difference between 10^{-11} and 10^{-12}). For larger problems LTFD seems to have an

advantage because of a) the smaller truncation error, equal to the truncation error of the space discretization only, and b)a smaller roundoff error due to fewer operations.

The material balance error of the LTFD method generally improved as N_S increased. We determined that a $12 \leq N_S \leq 16$ yields the smallest material balance error. However, for practical purposes, the improvement between $N_S = 6$ and $N_S = 20$ was marginal. The implications of these observations are that a) for $N_S \leq 20$ the accuracy of LTFD is practically insensitive to the value of N_S, and b) the number of summation terms N_S for an accurate solution may be far fewer than the $N_S = 18$ suggested by Stehfest[7] for double precision variables. Our experience in this area tends to suggest that the combination of the Finite Difference discretization with the Stehfest algorithm may act as a filter in the LTFD scheme , removing frequencies which could cause errors in the application of the Stehfest algorithm in the inversion of simple functions. In light of the extremely small mass balance error, we suggest a value of $6 \leq N_S \leq 10$ for LTFD simulations. This reduces significantly the execution time requirements.

The material balance error for LTFD method starts to deteriorate when $N_S > 16$. This is probably due to limitations imposed by the computer accuracy in the determination of the weighing factors V_ν in Eq. 35. The calculations involve operations with factorials, which may become inaccurate for large numbers. Although this deterioration may be eliminated in computers with more significant figures in double precision variables than was used in this study, this would be pointless and undesirable because Eq. 31 would have to be solved more times and would require longer execution times.

Conclusions

1. A new numerical method, the Laplace Transform Finite Difference (LTFD) method, was developed for the solution of the nonlinear, parabolic Partial Differential Equation (PDE) of transient, slightly compressible, single-phase liquid flow through porous media.

The nonlinearilty of the PDE is removed by using a variation of the density formulation, the ΔR formulation. Because LTFD uses a Laplace transform formulation to remove the time dependency and eliminate the need for time discretization, it allows an unlimited timestep size without loss of stability or accuracy.

2. To evaluate the LTFD method we investigated four Test Problems. LTFD requires solution of the resulting system of simultaneous equations N_S times, one for each of the N_S different approximations of the Laplace space variable s. In essence, this means that the solution at any time is obtained by solving the system of simultaneous equations in LTFD N_S times and algebraically combining the solutions. We established that a $6 \leq N_S \leq 10$ is sufficient to provide an extremely accurate solution. Although the accuracy increases with increasing N_S for $N_S \leq 16$, the improvement is marginal and insufficient to justify the additional execution time.

3. The disadvantage of having to solve the system of simultaneous equations 6 to 10 times for a single timestep is outweighed by a) an unlimited timestep size without any loss of accuracy, b) a superior accuracy, and c) a stable, non-increasing roundoff error. Therefore, calculations in a LTFD scheme are necessary only at the desired observation times, thus allowing 'snapshots' in time. On the other hand, in a standard FD method calculations are needed at all the intermediate times of the discretized time domain.

4. With a smaller timestep size and more timesteps, the FD solution tended to approach the LTFD solution. The LTFD method provided a solution generally more accurate than the FD solution for the same space discretization. This was expected because a) the elimination of the time discretization limited the truncation error to that of the space discretization only, and b) the roundoff error was reduced due to the limited number of operations needed. An unlimited timestep size with a stable, non-increasing error is thus possible.

5. The LTFD methoddoes not increase the computer memory requirement over a standard implicit FD method.

Nomenclature

Ad^*	=	flow coefficient defined in Eq. A-7
B	=	formation volume factor
Bd^*	=	flow coefficient defined in Eq. A-9
Cd^*	=	flow coefficient defined in Eq. A-8
C_t	=	$C_L + C_R$
C_L	=	fluid compressibility
C_R	=	rock compressibility
C_T	=	defined in Eq. 12
C_β	=	defined in Eq. 21
d°	=	x, y, z
d^*	=	X, Y, Z
g	=	gravitational acceleration
Gd^*	=	defined in Eq. A-10
h	=	formation thickness
I, J, K	=	gridblock indices in the FD and LTFD models
k	=	absolute permeability
L	=	length of horizontal well
MX	=	gridblocks in the x direction (similarly for y, z)
p	=	pressure
p_D	=	dimensionless pressure = $2\pi kh(p_0 - p)/(QB\mu)$
P_w	=	well pressure
q	=	volumetric flow rate per unit volume
$\tilde{q}$	=	mass flow rate per unit volume
$\ddot{q}$	=	defined in Eq. 22

Q = volumetric flow rate

r = radius

r_w = well radius

r_D = dimensionless radius = r/r_w

$R, \Delta R$ = defined in Eqs. 5 and 16

t = time

t_D = dimensionless time = $kt/(\pi\ \phi\ \mu\ c_t\ r_w^2)$

t_{DA} = dimensionless time = $kt/(4\phi\ \mu\ c_t\ x_e y_e)$

s = Laplace transform parameter

x_e = reservoir half length

x_f = fracture half length

y_e = reservoir half width

z = vertical coordinate

z_{d° = elevation gradient in the d° direction

β = $1/B$

δd° = $\frac{1}{2}\Delta d^\circ$

Δd° = Δx, Δy, Δz: Mesh spacing in x, y , and z

$\Delta d^\circ{}_{\kappa\pm1}$ = $\frac{1}{2}(\Delta d^\circ{}_\kappa + \Delta d^\circ{}_{\kappa\pm1})$

Δp = difference between the LTFD and the FD solution

Δt = timestep

Δt_{max} = maximum allowable timestep

$\Delta t_{\Delta pmax}$ = defined after Eq. 38

$\Delta\Psi$ = defined in Eq. A-2

κ = i, j, k

$\lambda_{d^\circ 1,2}$ = defined in Eq. 19

μ = dynamic viscosity

ρ = fluid density

ϕ = porosity

Ψ = defined in Eq. 23

Subscripts

0 = initial state

i, j, k = gridblock indices in the x, y , and z direction

STC = standard conditions

Acknowledgements

This work was supported by the Texas Agricultural Experiment Station under grant 6993/91, and the U.S. Department of Energy under Contract No. DE-AC03-76SF00098. The authors thank Drs. Curt Oldenburg and Sally Benson for their useful review comments.

Appendix – Derivation of the Flow Coefficients

Using a Taylor series, the d°-derivative ($d^\circ \equiv x, y, z$) on the left side of Eq. 20 is approximated by

$$\frac{\partial}{\partial d^\circ}\left[\lambda_{d^\circ 1}\frac{\partial \Psi}{\partial d^\circ} - \lambda_{d^\circ 2} C_\beta \Psi - \frac{\lambda_{d^\circ 2}}{s}\right]_\kappa \simeq$$

$$\frac{1}{\Delta d^\circ_\kappa}\left[(\lambda_{d^\circ 1})_{\kappa+\frac{1}{2}}\frac{\Delta\Psi^+}{\Delta d^\circ_{\kappa+\frac{1}{2}}} - \left(\lambda_{d^\circ 2} C_\beta \Psi + \frac{\lambda_{d^\circ 2}}{s}\right)_{\kappa+\frac{1}{2}} - (\lambda_{d^\circ 1})_{\kappa-\frac{1}{2}}\frac{\Delta\Psi^-}{\Delta d^\circ_{\kappa-\frac{1}{2}}} + \left(\lambda_{d^\circ 2} C_\beta \Psi + \frac{\lambda_{d^\circ 2}}{s}\right)_{\kappa-\frac{1}{2}}\right], \qquad (A-1)$$

where

$$\Delta\Psi^\pm = \Psi^\pm_{\kappa\pm 1} - \Psi_\kappa \ , \qquad (A-2)$$

$$(\lambda_{d^\circ 2} C_\beta \Psi)_{\kappa\pm\frac{1}{2}} = \frac{\delta d^\circ_\kappa}{\Delta d^\circ_{\kappa\pm\frac{1}{2}}} (\lambda_{d^\circ 2} C_\beta \Psi)_{\kappa\pm 1} + \frac{\delta d^\circ_{\kappa\pm 1}}{\Delta d^\circ_{\kappa\pm\frac{1}{2}}} (\lambda_{d^\circ 2} C_\beta \Psi)_\kappa \ , \qquad (A-3)$$

$$\left(\frac{\lambda_{d^\circ 2}}{s}\right)_{\kappa\pm\frac{1}{2}} = \frac{\delta d^\circ_\kappa}{\Delta d^\circ_{\kappa\pm\frac{1}{2}}} (\lambda_{d^\circ 2})_{\kappa\pm 1} \cdot \frac{1}{s} + \frac{\delta d^\circ_{\kappa\pm 1}}{\Delta d^\circ_{\kappa\pm\frac{1}{2}}} (\lambda_{d^\circ 2})_\kappa \cdot \frac{1}{s} \ , \qquad (A-4)$$

and

$$\kappa \equiv \begin{cases} i & \text{if } d^\circ \equiv x \\ j & \text{if } d^\circ \equiv y \\ k & \text{if } d^\circ \equiv z \end{cases} .$$

The subscript $\kappa \pm \frac{1}{2}$ refers to the interblock value of the quantity involved.

Calculation of the exact pressure drop between grid-blocks κ and $\kappa \pm 1$ ($\kappa \equiv i, j, k$) in the FD scheme leads to the determination of $\lambda_{d^\circ 1}$ at $\kappa \pm \frac{1}{2}$ as

$$(\lambda_{d^\circ 1})_{\kappa\pm\frac{1}{2}} = \frac{\delta d^\circ_\kappa + \delta d^\circ_{\kappa\pm 1}}{\dfrac{\delta d^\circ_\kappa}{(\lambda_{d^\circ 1})_\kappa} + \dfrac{\delta d^\circ_{\kappa\pm 1}}{(\lambda_{d^\circ 1})_{\kappa\pm 1}}}, \quad d^\circ \equiv x, y, z \ . \qquad (A-5)$$

Therefore, $(\lambda_{d^\circ 1})_{\kappa\pm\frac{1}{2}}$ is the harmonic mean value of $(\lambda_{d^\circ 1})$ of the adjacent grid-blocks. Eq. A-5 minimizes the mass balance error. Eq. A-1 is then written as:

$$\frac{\partial}{\partial d^\circ}\left[\lambda_{d^\circ 1}\frac{\partial \Psi}{\partial d^\circ} - \lambda_{d^\circ 2} C_\beta \Psi - \frac{\lambda_{d^\circ 2}}{s}\right]_\kappa \simeq$$

$$Ad^*_\kappa \cdot \Psi_{\kappa-1} + Bd^*_\kappa \cdot \Psi_\kappa + Cd^*_\kappa \cdot \Psi_{\kappa+1} + Gd^*_\kappa \ , \qquad (A-6)$$

where

$$Ad^*_\kappa = \frac{(\lambda_{d^\circ 1})_{\kappa-\frac{1}{2}} - \delta d^\circ_{\kappa-1} \cdot (\lambda_{d^\circ 2} C_\beta)_{\kappa-1}}{\Delta d^\circ{}_\kappa \cdot \Delta d^\circ{}_{\kappa-\frac{1}{2}}} \ , \qquad (A-7)$$

$$Cd^*_\kappa = \frac{(\lambda_{d^\circ 1})_{\kappa+\frac{1}{2}} - \delta d^\circ_{\kappa+1} \cdot (\lambda_{d^\circ 2} C_\beta)_{\kappa+1}}{\Delta d^\circ{}_\kappa \cdot \Delta d^\circ{}_{\kappa+\frac{1}{2}}} \ , \qquad (A-8)$$

$$Bd^*_\kappa = -(Ad^*_\kappa + Cd^*_\kappa) \ , \qquad (A-9)$$

$$Gd^*_\kappa = \frac{1}{\Delta d^\circ{}_\kappa}\left[\left(\frac{\lambda_{d^\circ 2}}{s}\right)_{\kappa-\frac{1}{2}} - \left(\frac{\lambda_{d^\circ 2}}{s}\right)_{\kappa+\frac{1}{2}}\right], \qquad (A-10)$$

and $d^* \equiv X, Y, Z$.

References

1. Moridis, G.J., and Reddell, D.L.:"The Laplace Transform Finite Difference (LTFD) Numerical Method for Groundwater Simulations",paper H52B-01 presented at the 1990 AGU Spring Meeting, Baltimore, May 27-30, *EOS Trans. of AGU* (May 1990), **71**, No. 17.
2. Moridis, G.J., and Reddell, D.L.:"The Laplace Transform Finite Difference Method for Simulation of Flow Through Porous Media", *Water Resour. Res.* (1991) **27**, No. 8, 1873-1884.
3. Moridis, G.J., and Reddell, D.L.:"The Laplace Transform Finite Difference (LTFD) Numerical Method for the Simulation of Solute Transport in Groundwater", paper H42A-07 presented at the 1990 AGU Fall Meeting, San Fransisco, Dec. 3-7, *EOS Trans. of AGU* (May 1990), **71**, No. 43.
4. Moridis, G.J., and Reddell, D.L.:"The Laplace Transform Boundary Element (LTBE) Numerical Method for the Solution of Diffusion-Type Equations", in *Boundary Elements XIII*, Proc. 13th Boundary Element Method International Conference, Tulsa (1991), C.A. Brebbia and G.C. Gibson (eds.), Computational Mechanics Publications and Elsevier applied Sciences, London (1991), 83-97.
5. Moridis, G.J., and Reddell, D.L.:"The Laplace Transform Finite Element (LTFE) Numerical Method for the Solution of the Groundwater Equation Groundwater Simulations", paper H22C-04 presented at the 1991 AGU Spring Meeting, Baltimore, May 27-30, *EOS Trans. of AGU* (April 1991), **72**, No. 17..
6. Aziz, K., and Settari, A.: *Petroleum Reservoir Simulation*,Elsevier Applied Science

Publishers, New York (1979) 69-80. 476 pp., Elsevier Science, New York, 1979

7. Stehfest, H.: "Numerical Inversion of Laplace Transforms", *Communications of the ACM* (Jan. 1970), **13**, No. 1, Algorithm 368, 47-49.
8. Stehfest, H.: "Numerical Inversion of Laplace Transforms", *Communications of the ACM* (Jan. 1970), **13**, No. 10, Algorithm 368, 56.
9. *SABRE- A General Purpose Three-Dimensional, Three-Phase Petroleum Reservoir Simulator, User's Manual*, Version 2.00, S. A. Holditch & Associates, College Station (October 1989)
10. van Everdingen, A.F., and Hurst, W.: "The Application of the Laplace Transformation to Flow Problems in Reservoirs", Trans., AIME(1949) 186, 305-324.
11. Gringarten, A.C., Ramey, H.J., Jr., ann Raghavan, R.: "Unsteady-State Pressure Distributions Created by a Well with a Single Infinite Conductivity Vertical Fracture, SPEJ (August 1974) 347-360.

SI Metric Conversion Factors

bbl	× 1.589873	E-01	= m^3
cp	× 1.0	E-03	= Pa·s
ft	× 3.048	E-01	= m
md	× 9.869233	E-04	= μm^2
psi	× 6.894757	E+00	= kPa

TABLE 1 - TIME DISCRETIZATION FOR THE FD METHOD

Test Problem #	Δt_0 (days)	Δt_{max} (days)	M_L	Δ_{pmax} (psi)	Num. of Δt	Num. of MS
1	60	60	1	3000	1	3
	10	30	5	1000	3	9
	0.1	10	5	500	9	23
	0.001	1	5	250	65	136
2	100	365	5	1000	3	11
	20	100	2	500	6	18
	0.1	50	3	500	13	36
	0.001	5	5	250	79	231
3	1	100	5	1000	10	39
	0.1	50	5	500	18	59
	0.01	25	5	500	21	68
	0.01	2	5	250	86	329
4	0.01	1000	5	500	24	73
	0.01	100	5	500	27	82
	0.01	50	5	500	34	102
	0.01	10	5	250	133	399
	0.001	5	5	250	231	680

MS: Matrix solution

TABLE 2 - FLUID PROPERTIES IN TEST PROBLEM 1

p	5000 psi
B	1.2
μ	1 cp
C_L	1.5×10^{-5} psi^{-1}

TABLE 3 - RESERVOIR PROPERTIES, GEOMETRY, AND DISCRETIZATION IN TEST PROBLEM 1

	ϕ	0.15
	k	10 md
	C_R	0.0 psi^{-1}
	h	30 ft
	Q	50 bbl/D
	r_w	0.25 ft
	r_e	2,500 ft
Discretization		
MX	62	
Δr (in ft)	0.00033,0.00066,0.00131,0.00262,0.00328, 0.0105,0.021,0.042,0.084,0.168,0.336, 0.672,1.3438,2.6877,3.281,3.281,4.921, 7.382,11.073,16.609,24.934,37.139,53.077, 82.02,82.02,82.02,82.02,82.02,82.02,82.02, 82.02,82.02,82.02,82.02,82.02,82.02,82.02, 82.02,82.02,82.02,82.02,82.02,82.02,82.02, 82.02,82.02,82.02,65.617,65.617,65.617, 49.213,32.81,32.81,16.4,16.4,9.843,6.562, 3.28,1.64,0.984,0.328,0.164,0.164	

TABLE 4 - RESERVOIR PROPERTIES, GEOMETRY, AND DISCRETIZATION IN TEST PROBLEM 2

ϕ		0.15
$k_x = k_y$		10 md
k_x along x_f (I=1-26, J=1)		10^7 md
C_R		0.0 psi^{-1}
h		30 ft
Q		50 bbl/D
$x_e = y_e$		1000 ft
x_f		500 ft
Discretization		
MX	40	
Δx (in ft)	0.005,0.02,0.025,0.05,0.25,0.25,0.5,1.5 2.5,7.5,15,25,25,50,50,50,50,50,50,40, 30,20,15,10,5,2.5,2.5,5,10,15,20,30,40, 50,50,50,50,50,50,77.5	
MY	24	
Δy (in ft)	0.001,0.004,0.015,0.03,0.05,0.1,0.3,0.5, 1,3,5,10,20,30,50,80,100,100,100,100, 100,100,100,100	

TABLE 5 - RESERVOIR PROPERTIES, GEOMETRY, AND DISCRETIZATION IN TEST PROBLEM 3

	ϕ	0.10
	k	Variable (Fig. 8b)
	C_R	0.0 psi^{-1}
	h	Variable (Fig. 8a)
Discretization		
MX	48	
Δx (in ft)	48x200 (uniform size)	
MY	36	
Δy (in ft)	36x200 (uniform size)	

TABLE 6 - WELL INFORMATION IN TEST PROBLEM 3

General well rate equation: $Q = Q_0 + Q_1 t + Q_2 \exp(-Q_3 t)$

Well Location I	J	Q_0 (bbl/D)	Q_1 (bbl/D)	Q_2 (bbl/D)	Q_3 (bbl/D)
6	17	-15	0.0041	0	0
14	18	-10	0	0	0
17	25	-10	0	-50	0.0037851
22	15	-15	0	-60	0.0189254
26	25	-20	0	-45	0.0037851
28	8	-10	0	0	0
31	14	-15	0	-30	0.0037851
33	21	-40	0.0137	0	0
38	17	-20	0.0055	0	0
42	27	-10	0	0	0

TABLE 7 - RESERVOIR PROPERTIES, GEOMETRY, AND DISCRETIZATION IN TEST PROBLEM 4

ϕ	0.15
k_x	10 md
k_y	3 md
k_z	0.001 md
C_R	0.0 psi^{-1}
P_w	1000 psi
L	1000 ft
Dimensions in x,y,z (ft)	2640 x 2640 x 31.75

Discretization

MX	26
Δx (in ft)	5x141,140,80,40,20,10,5,5,10,20,40,80, 9x148,153
MY	14
Δy (in ft)	0.25,0.5,1,2,4,8,16,32,64,128,256,512, 2x808.13
MZ	7
Δy (in ft)	0.25,0.5,1,2,4,8,16

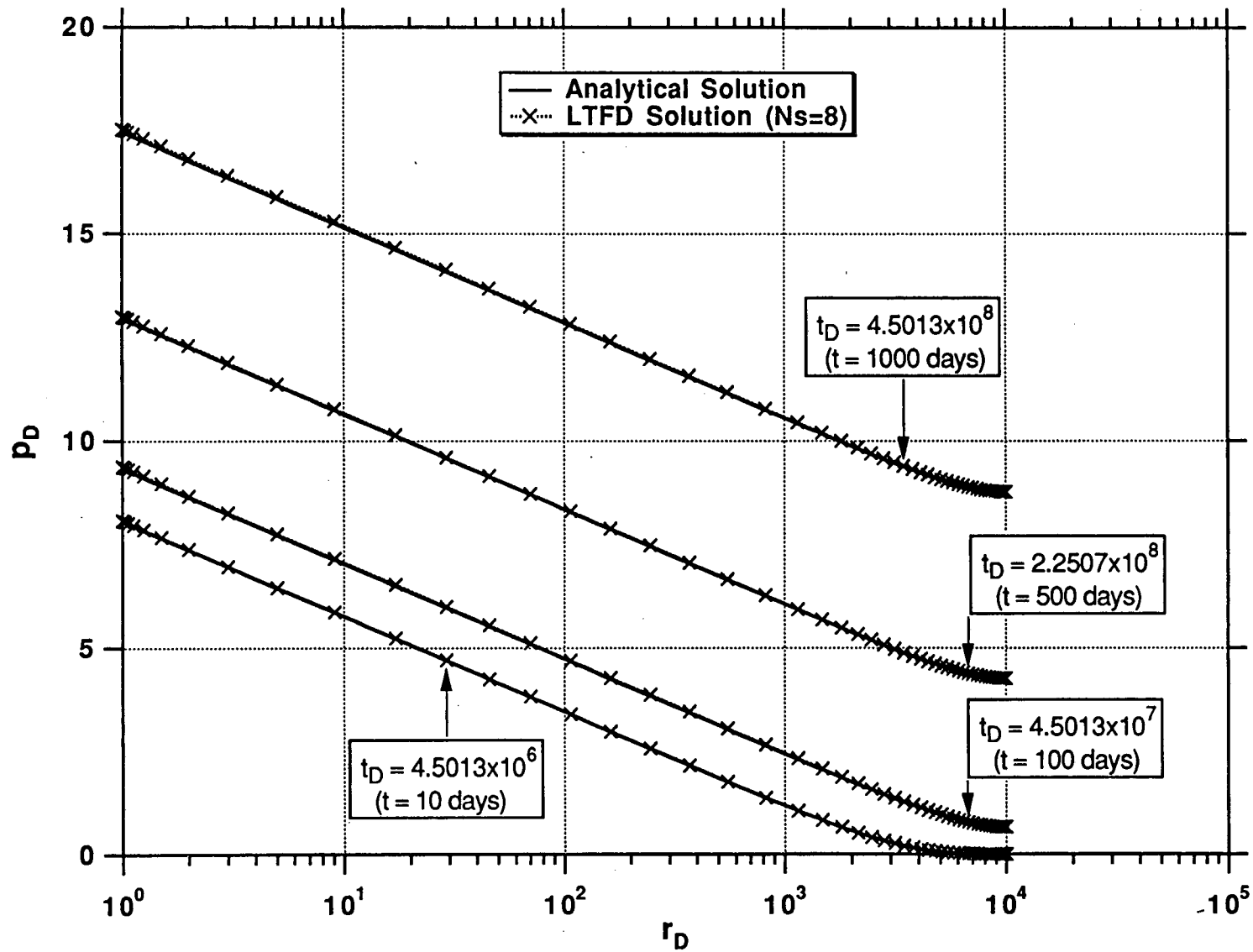

Fig. 1 - Comparison of analytical and LTFD solutions of p_D for various t_D's-Test Problem 1a.

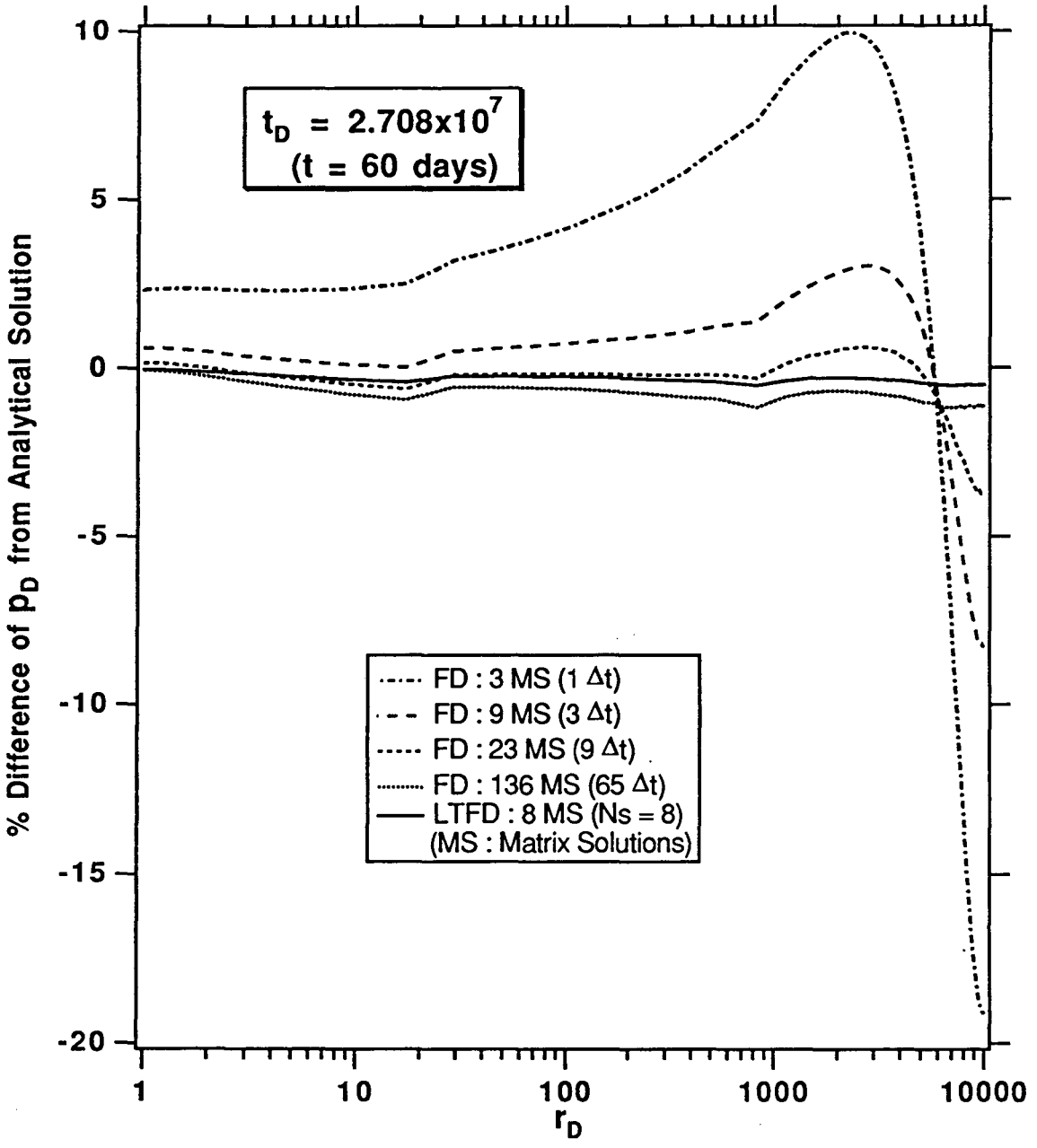

Fig. 2 - % Difference of the LTFD and the FD solutions of p_D from the analytical solution for t_D = 2.708x10^7 (t = 60 days) - Test Problem 1b.

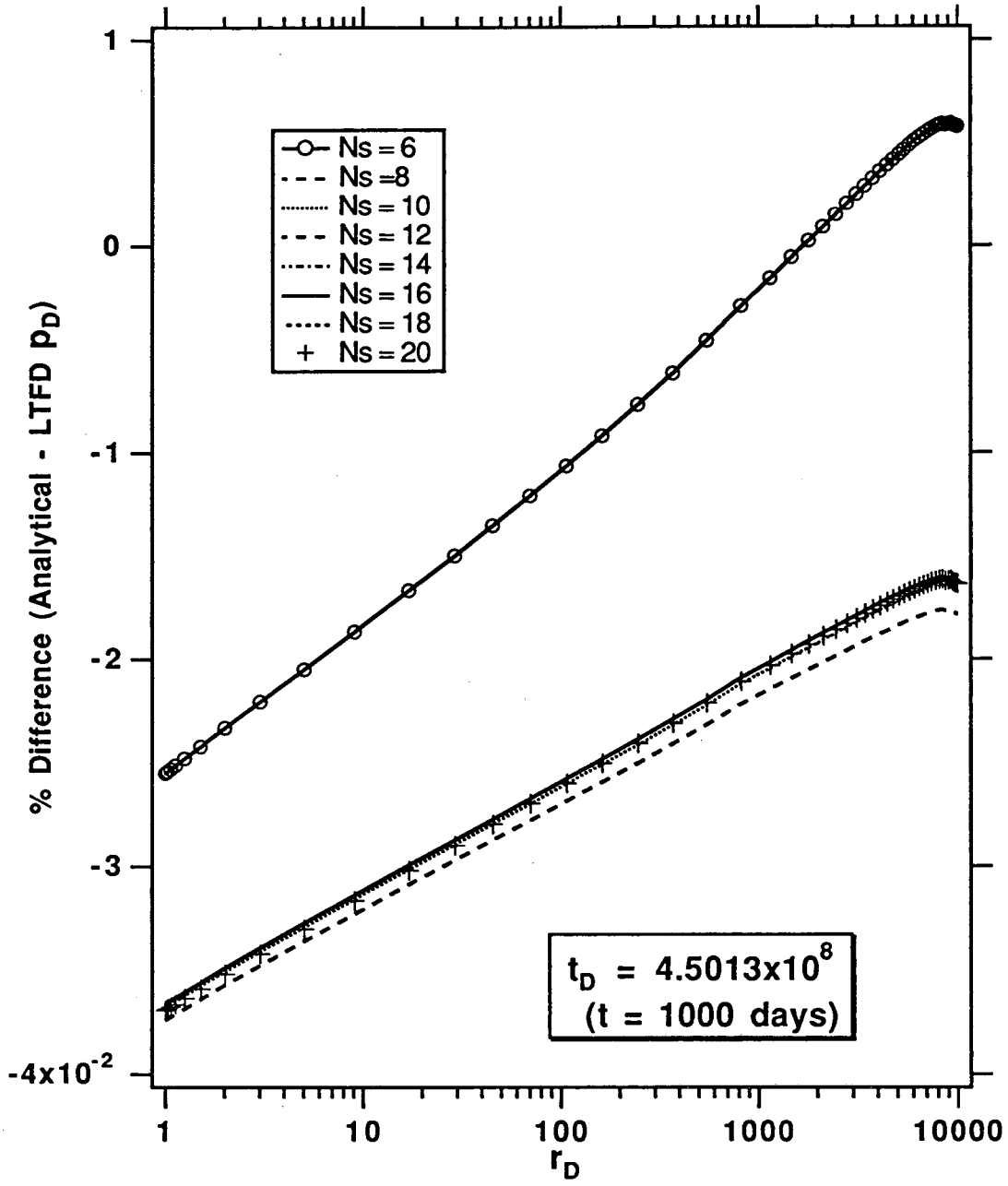

Fig. 3 - Effect of Ns on the difference (%) of the LTFD solution from the analytical solution of p_D for $t_D = 4.5013 \times 10^8$ (t = 1000days) - Test Problem 1c.

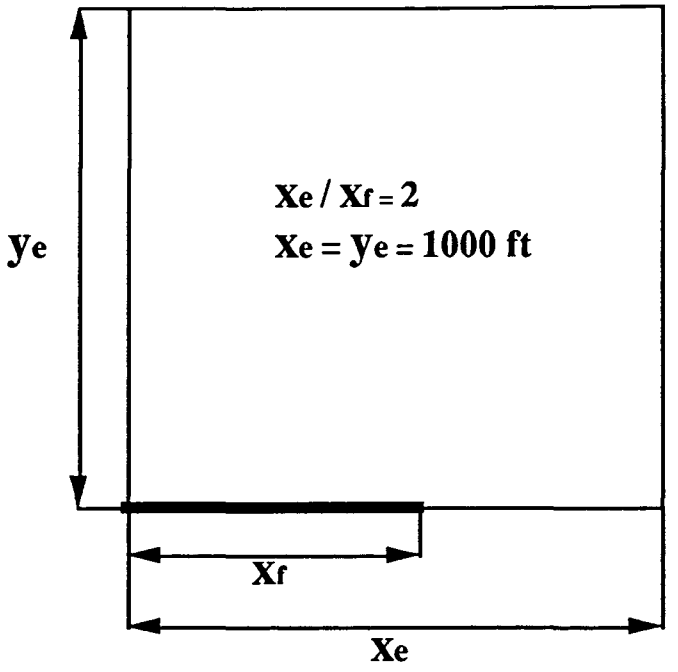

Fig. 4 - Geometry of Test Problem 2-A square reservoir with an infinite-conductivity fracture at the center. A quarter of the reservoir (shown) was modeled.

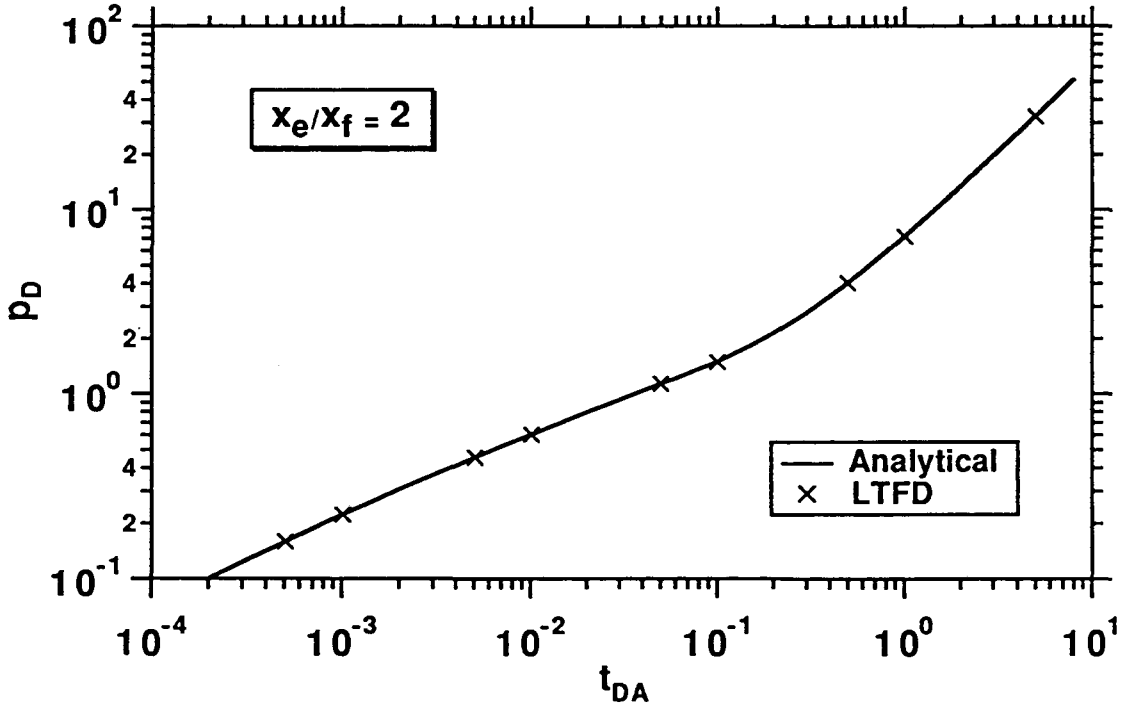

Fig. 5 - Comparison of the analytical and the LTFD solutions of p_D for various t_{DA}'s-Test Problem 2a.

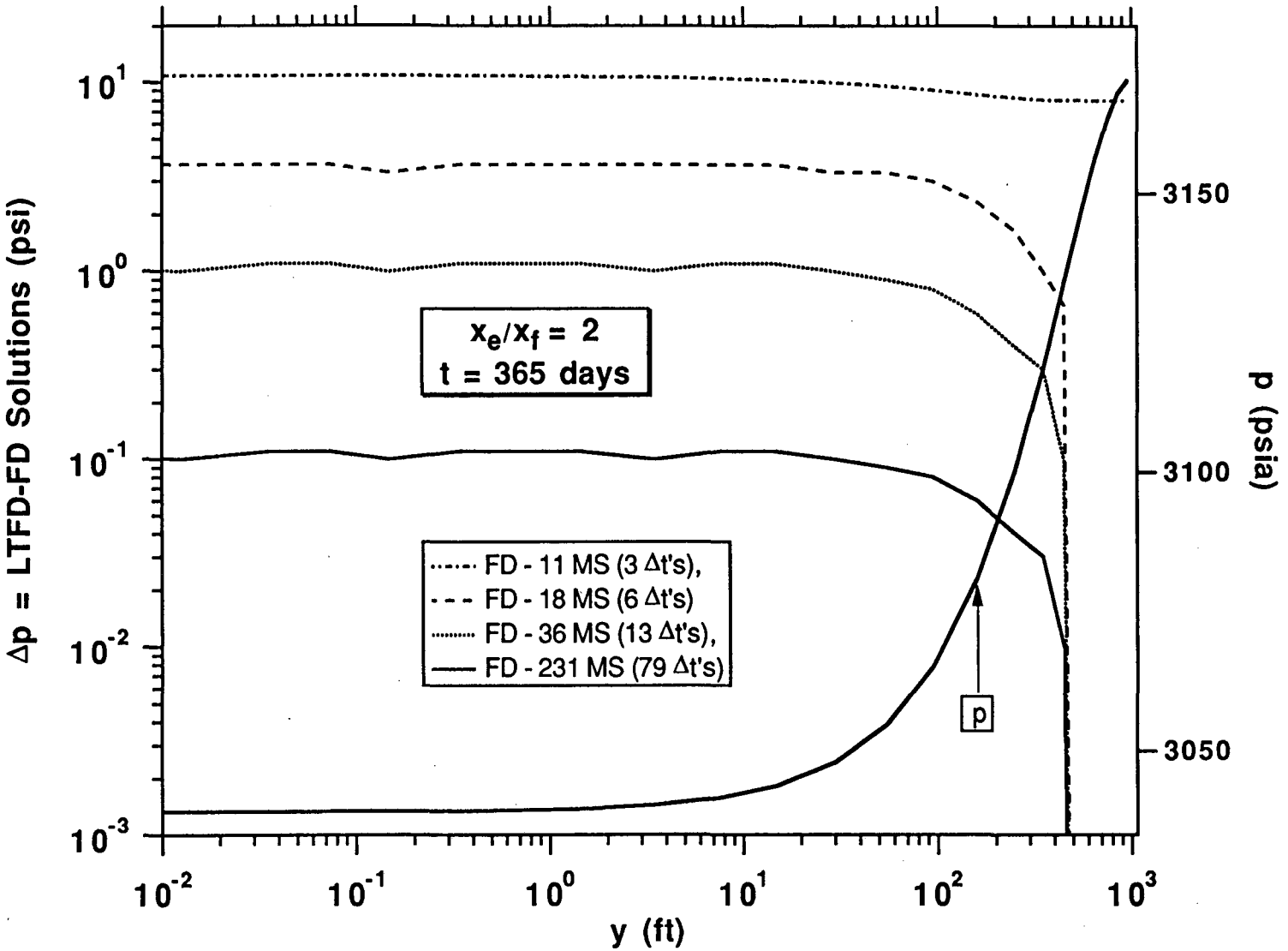

Fig. 6 - Test Problem 2b-Difference Δp between the LTFD and the FD solutions along y at x=0.025 ft (l=1), t=365 days. The pressure distribution along the same axis is shown.

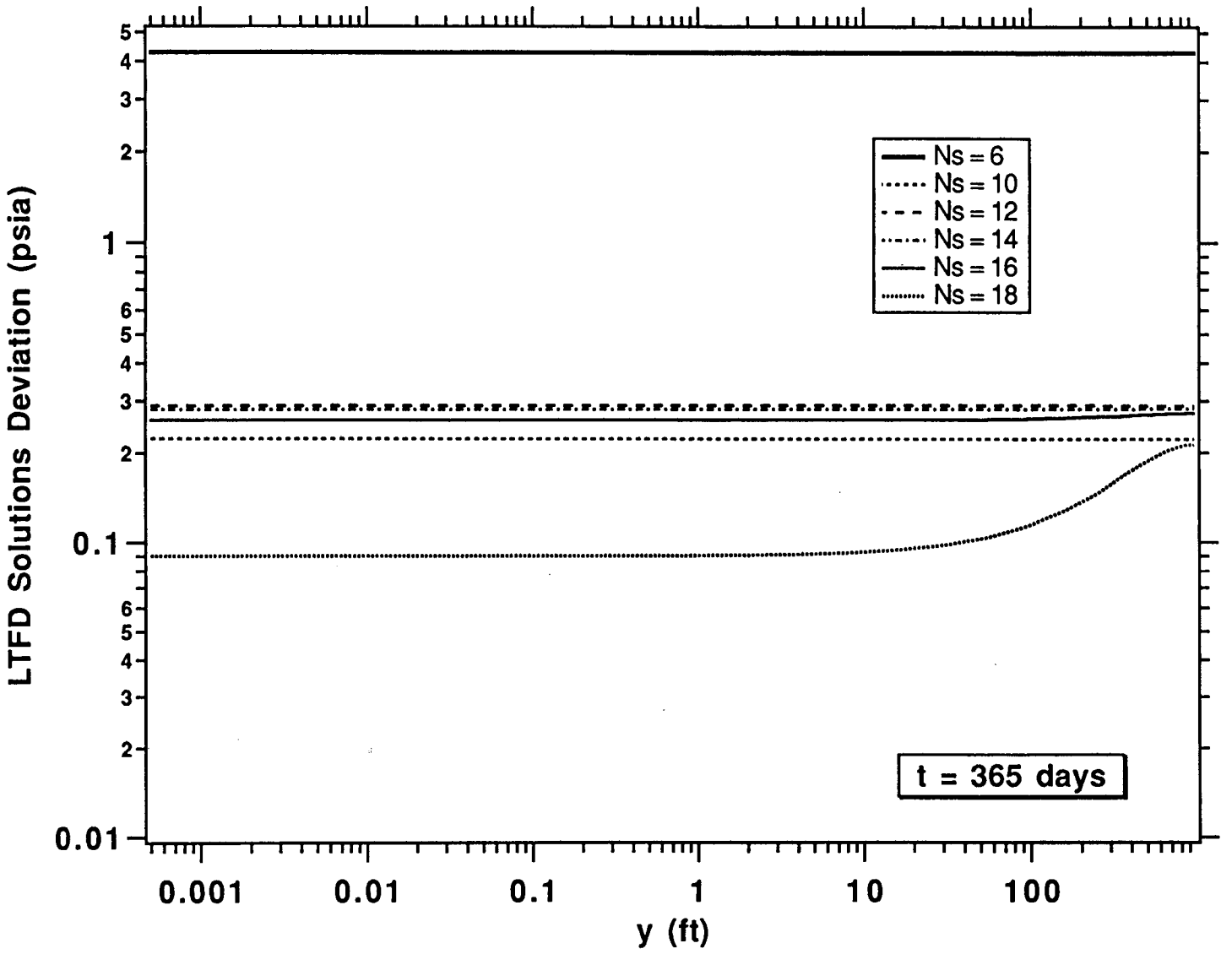

Fig. 7 - Effect of Ns on the performance of LTFD, indicated by the absolute difference of the LTFD solutions for Ns = 6,...,18 from the LTFD solution for Ns = 8 - Test Problem 2c.

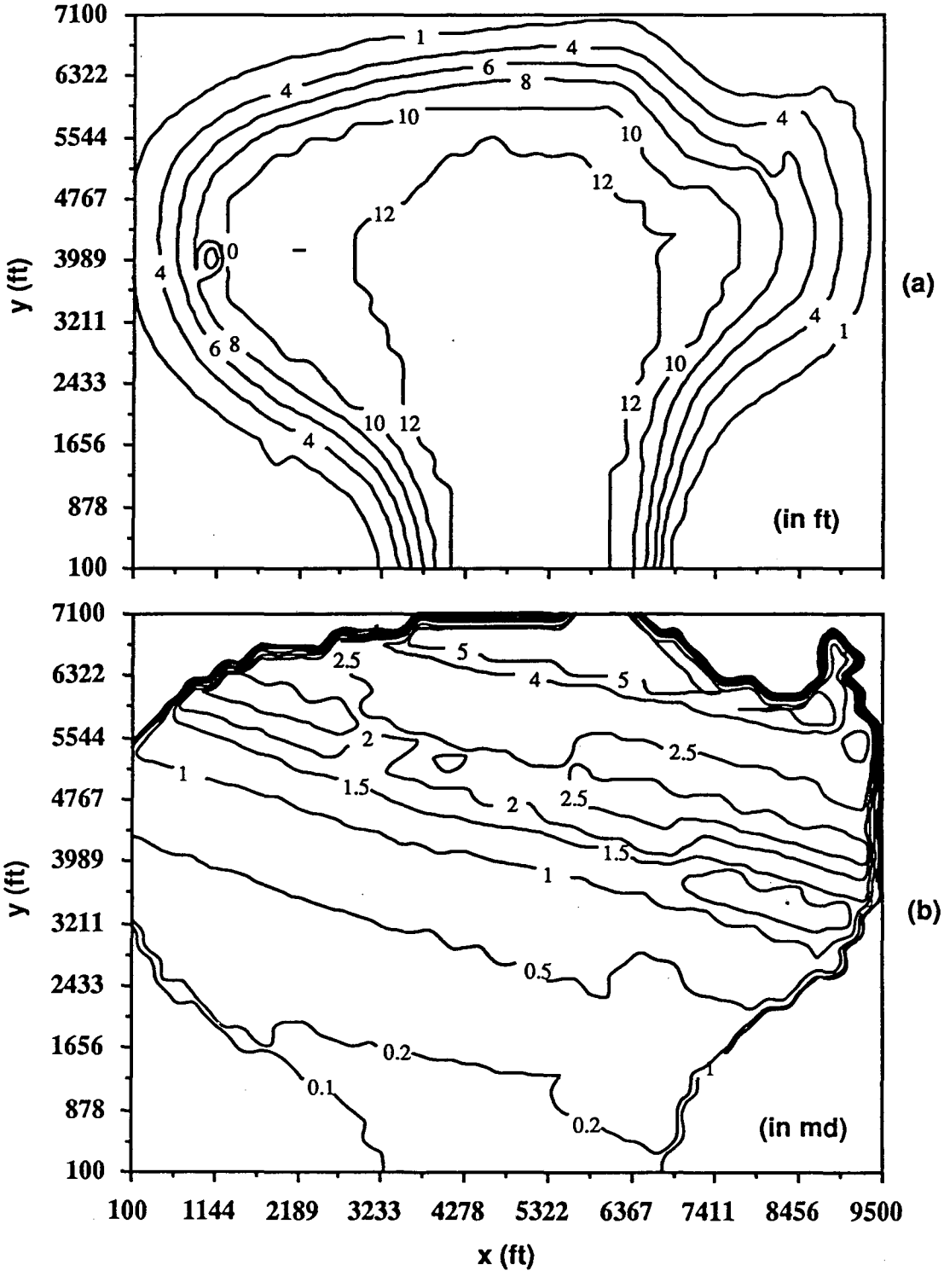

Fig. 8 - Reservoir geometry and property profile of the reservoir in Test Problem 3: (a) formation thickness, (b) permeability.

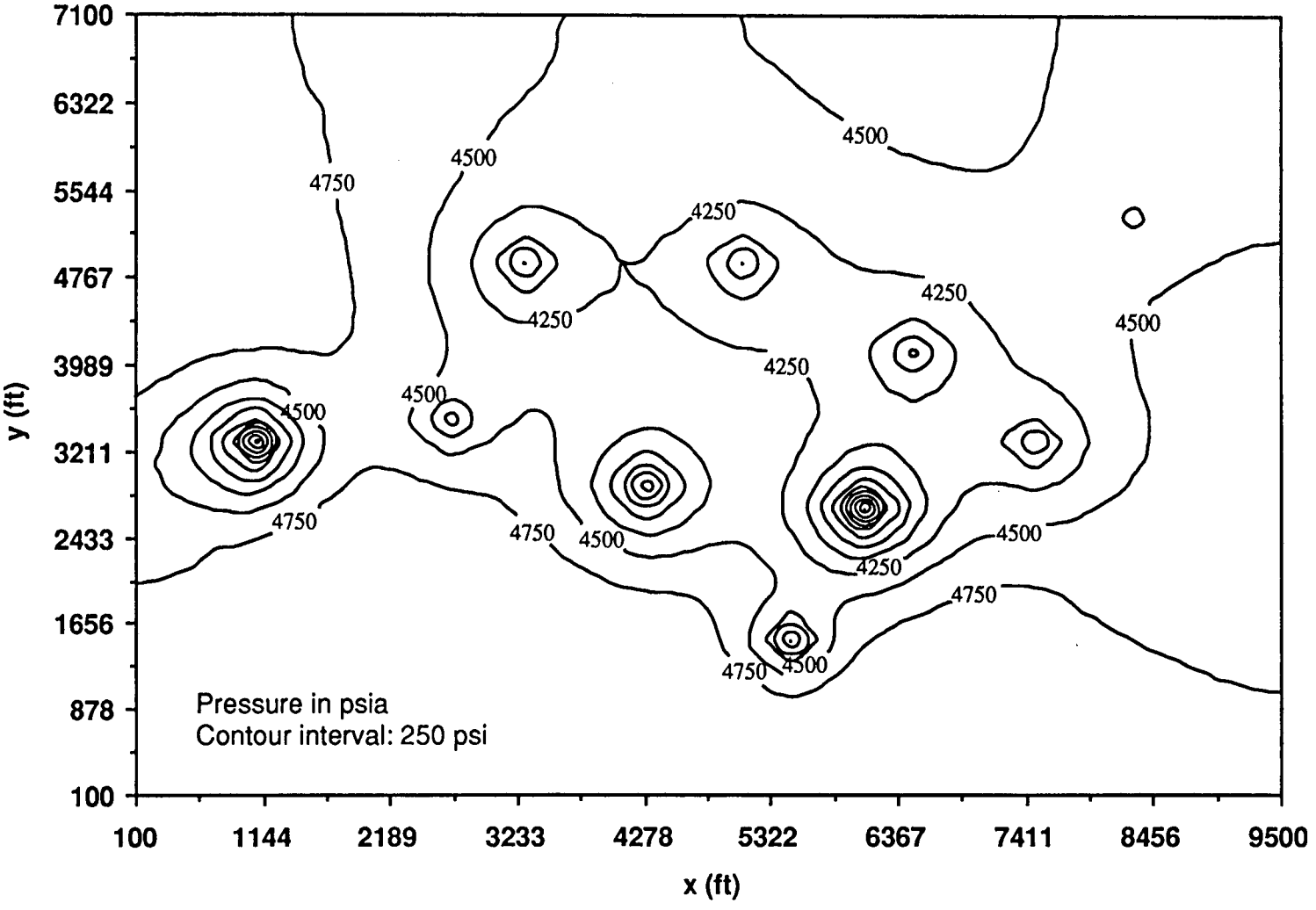

Fig. 9 - LTFD solution of pressure distribution in the reservoir at t = 180 days-Test Problem 3.

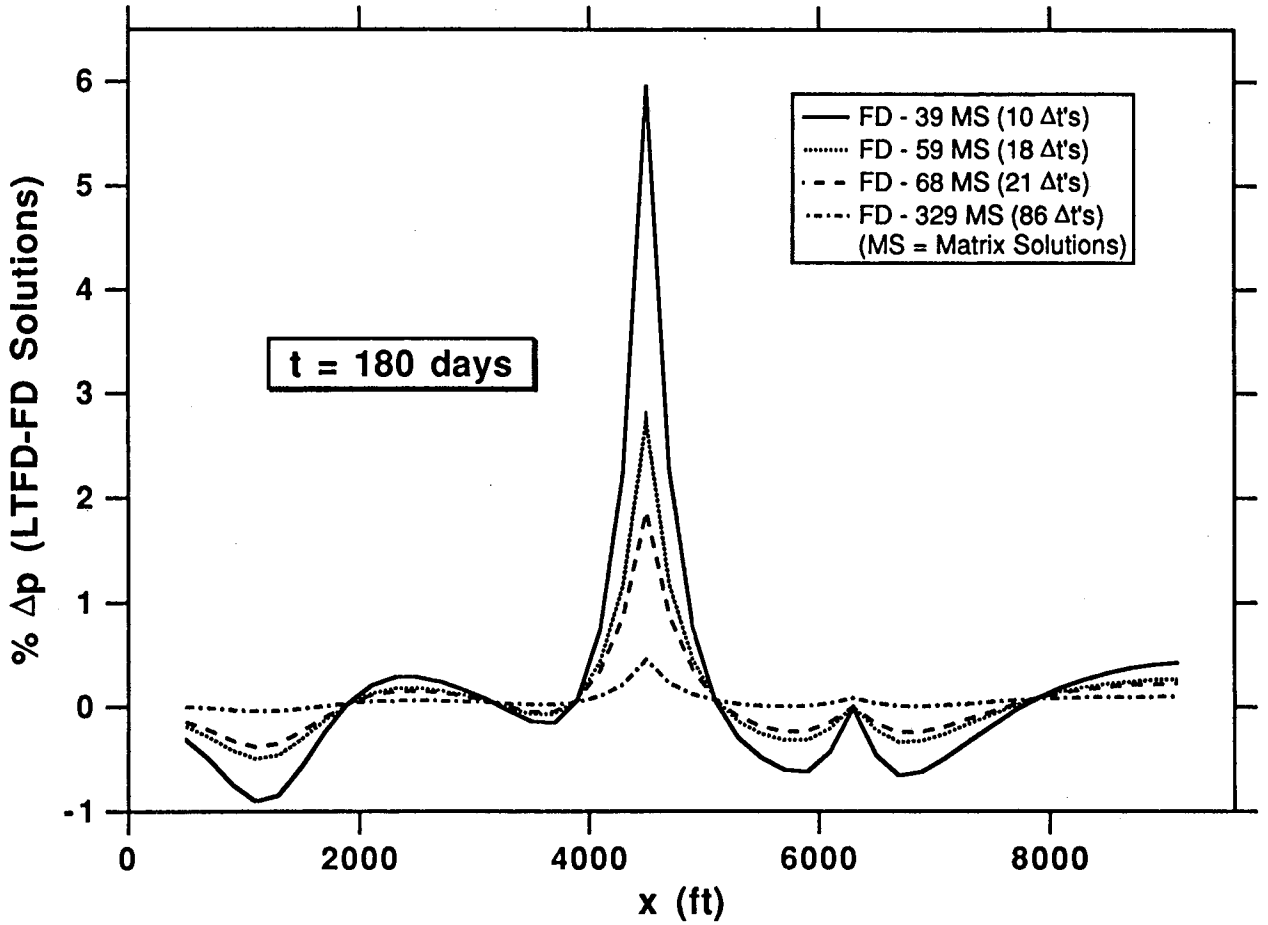

Fig. 10 - Difference (%) Δp between the LTFD and the FD solutions along x at y=2900 ft (J=15), t=180 days - Test Problem 3.

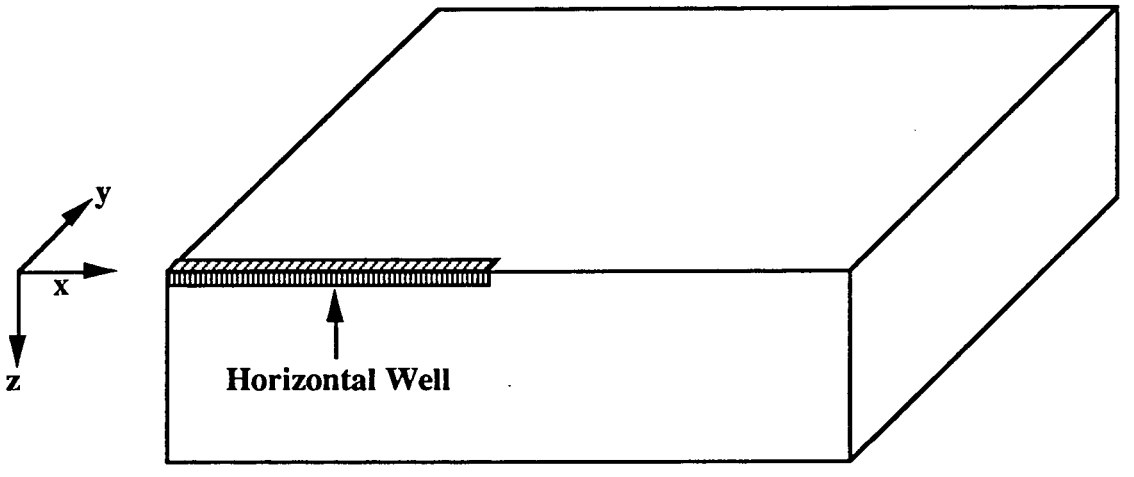

Fig. 11 - Geometry and position of the horizontal well in the reservoir of Test Problem 4.

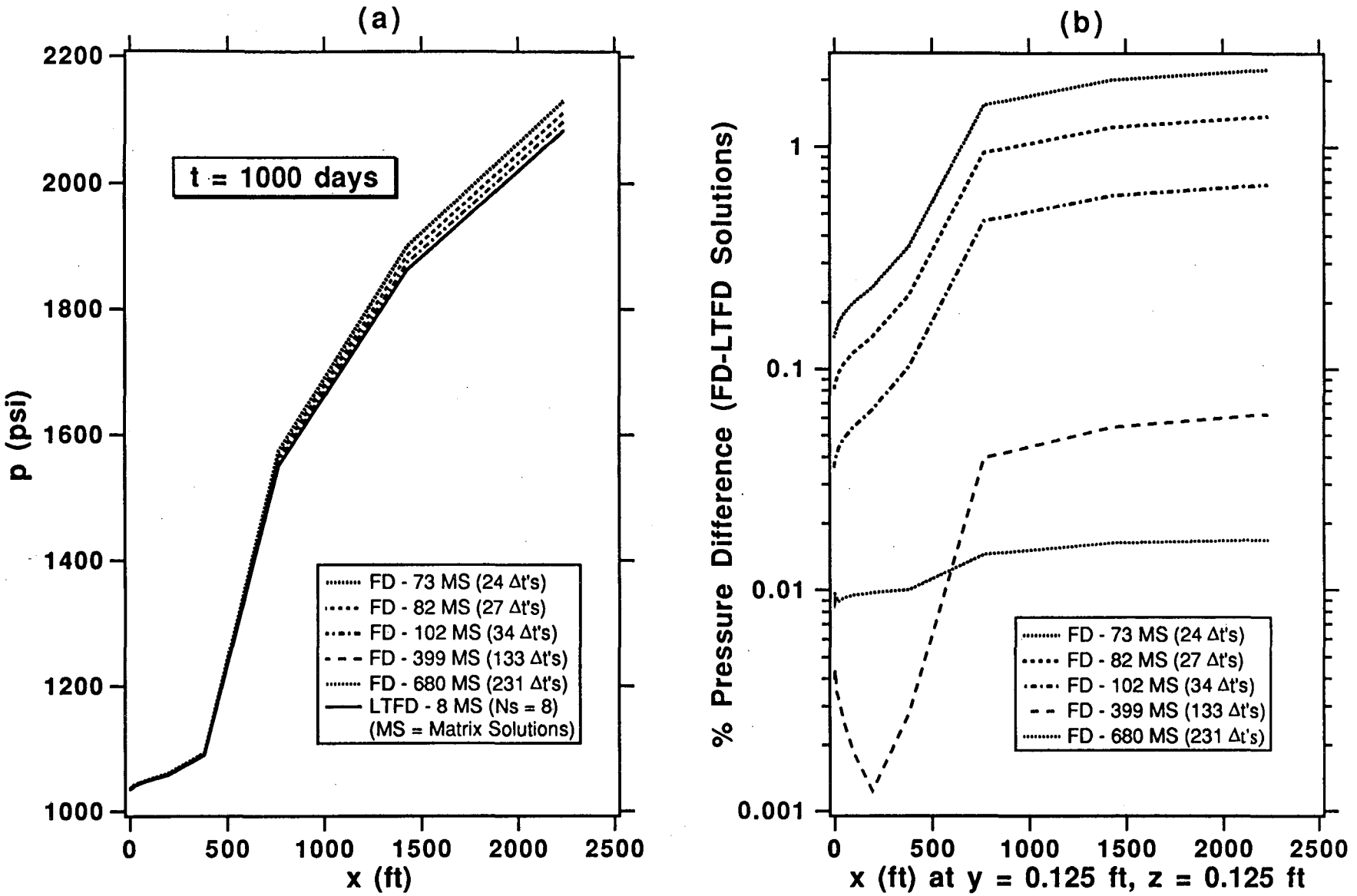

Fig. 12 - Comparison of the LTFD and the FD solutions along x at y = 0.125 ft (J=2), z= 0.125 ft (K=2) and for t=1000 days: (a) Pressures, and (b) % difference of the FD solutions from the LTFD pressure solution -Test Problem 4.

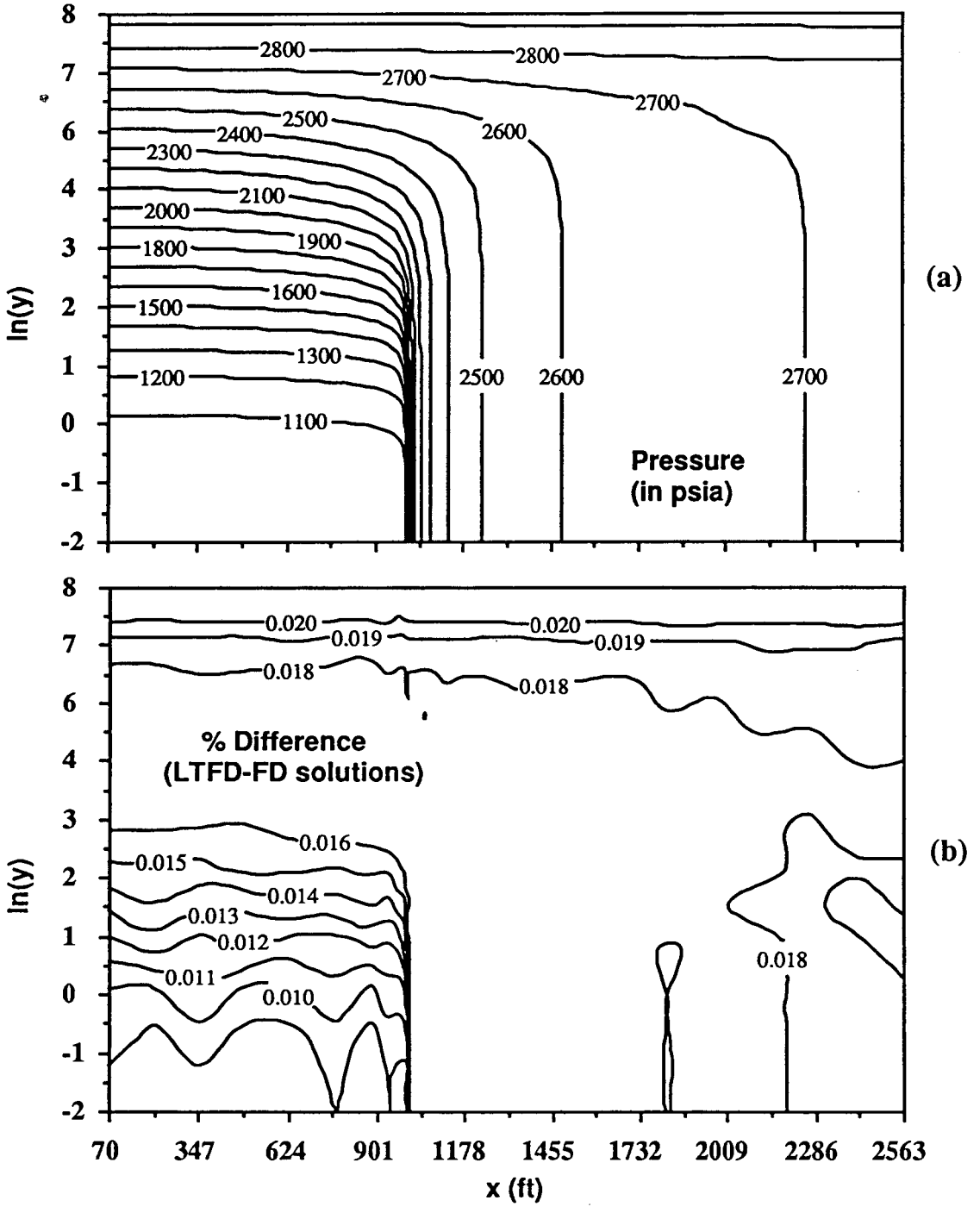

Fig. 13--Comparison of the LTFD and FD solutions on the xy plane at z = 0.125 ft (K=1): (a) the pressure distributions virtually coincide when FD uses 231 timesteps, as shown by the % difference between the two solutions in (b)-Test Problem 4.

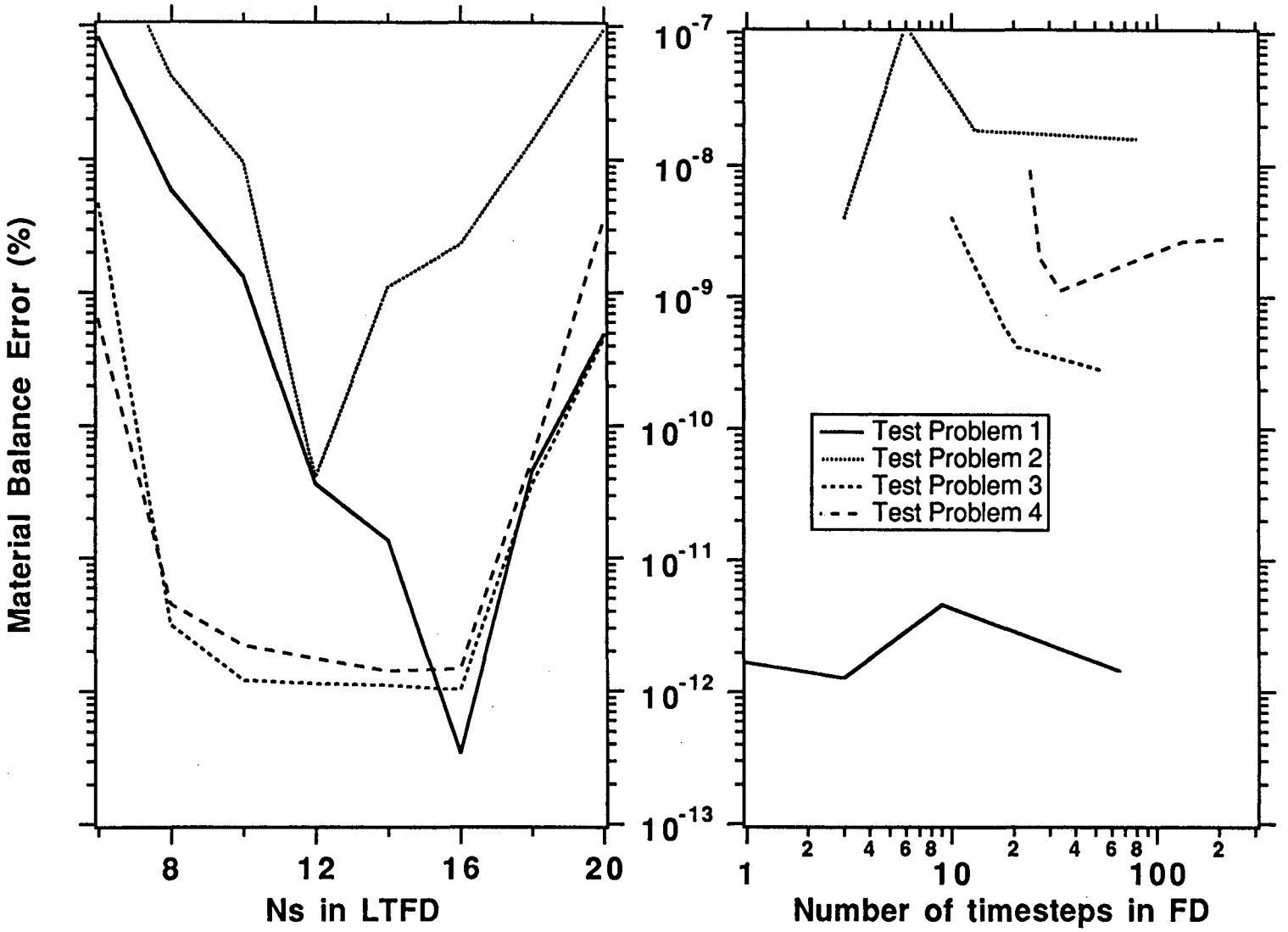

Fig. 14 - Material balance errors of the 4 Test Problems: (a) LTFD; (b) FD.

LAWRENCE BERKELEY LABORATORY
UNIVERSITY OF CALIFORNIA
TECHNICAL INFORMATION DEPARTMENT
BERKELEY, CALIFORNIA 94720